

Deep Learning Waveform Modeling for Wideband Optical Fiber Channel Transmission: Challenges and Potential Solutions

Minghui Shi*, Hang Yang*, Zekun Niu, Chuyan Zeng, Junzhe Xiao, Yunfan Zhang, Zhixiong Zheng, Weisheng Hu, and Lilin Yi

Abstract—Fast and accurate optical fiber communication simulation systems are crucial for optimizing optical networks, developing digital signal processing algorithms, and performing end-to-end (E2E) optimization. Deep learning (DL) has emerged as a valuable tool to reduce the complexity of traditional waveform simulation methods, such as the split-step Fourier method (SSFM). DL-based schemes have achieved high accuracy and low complexity fiber channel waveform modeling as its strong nonlinear fitting ability and high efficiency in parallel computation. However, DL-based schemes are mainly utilized in single-channel and few-channel wavelength division multiplexing (WDM) systems. The applicability of DL-based schemes in wideband WDM systems remains uncertain due to the lack of comparison under consistent standards and scenarios. In this paper, we propose a DSP-assisted accuracy evaluation method to evaluate the performance for DL-based schemes, from the aspects of waveform and quality of transmission (QoT) errors. We compare the performance of five various DL-based schemes and validate the effectiveness of the DSP-assisted method in WDM systems. The results suggest that feature-decoupled distributed (FDD) achieves better accuracy, especially in high-rate and large-channel scenarios. Furthermore, we find that the accuracy of FDD still exhibits significant degradation with the number of WDM channels and transmission rates exceed 15 and 100 GBaud, indicating challenges for wideband applications. We further analyze the reasons for performance degradation from the perspective of increased linearity and nonlinearity and discuss potential solutions including further decoupling scheme designs and improvement in DL models. Despite the remaining challenges of DL-based schemes in wideband WDM systems, they have strong potential for high-accuracy and low-complexity optical fiber channel waveform modeling. We believe that with further development, DL approaches will overcome these limitations, emerging as a novel tool for fast and accurate optical fiber channel simulation and facilitating the design of next-generation optical transmission systems.

Index Terms—Deep learning (DL), optical fiber channel modeling, waveform-level simulation, wideband wavelength division multiplexing (WDM) system.

I. INTRODUCTION

THE rapid expansion of technologies such as large language models (LLMs), autonomous driving, 5G+, and cloud computing has substantially increased the demand for wideband optical fiber transmission. [1]–[3]. Accurate and rapid optical fiber transmission simulation systems are critical for optimizing optical networks [4]–[9], advancing digital signal processing (DSP) algorithms [10]–[14], and performing end-to-end (E2E) optimization [15]–[21].

The Nonlinear Schrödinger Equation (NLSE) serves as the foundational framework for understanding optical signal evolution within fiber channels [22]. The classical numerical simulation method employs the split-step Fourier method (SSFM) [23], which divides the entire optical fiber link into multiple small segments and addresses the linear and nonlinear effects separately in each segment. However, SSFM requires numerous iterations, especially for wideband and long-haul optical fiber transmission to meet enough accuracy, leading to extremely high computational complexity and time consumption. Specifically, the computational complexity of SSFM typically scales to the fourth power of the bandwidth [24], resulting in simulation times of several hours for a single parameter. In this case, wideband simulation based on SSFM poses significant challenges for the deployment of next-generation wideband wavelength division multiplexing (WDM) systems.

Gaussian noise (GN) [25] and enhanced GN (EGN) [26] models provide the alternative fast simulation techniques, focusing primarily on power-level simulation, treats fiber nonlinearities as Gaussian noise and can estimate the generalized signal-to-noise ratio (GSNR). However, despite its utility in predicting system GSNR, the GN-like models are failed to provide signal waveform information, limited on some DSP applications such as nonlinearity compensation.

Recently, deep learning (DL) techniques have garnered attention for optical fiber channel modeling due to their superior nonlinear fitting capabilities [27] and efficiency in parallel computation [28]. DL-based schemes have demonstrated the potential to balance speed and accuracy in optical fiber communication and nonlinear photonics. Techniques such as bidirectional long short-term memory (BiLSTM) [29], conditional generative adversarial network (CGAN) [30], Fourier neural operator (FNO) [31], [32], multi-head attention mechanism [33], and center-oriented LSTM (Co-LSTM) [34] have been successfully applied in intensity modulation and direct detection (IM/DD) and coherent optical transmission systems. Additionally, physics-informed neural operators (PINO) [35] integrate physical principles into loss functions, reducing dataset dependency and enhancing training efficiency. For multi-channel WDM systems, full connected neural networks (FCNN) [36] and FNO [37] have been applied to few-channel WDM systems. A BiLSTM-based feature decoupled distributed (FDD) [38]–[40] scheme and a deep operator network (DeepONet) [41], [42] scheme have been extended

to wideband WDM configurations. DL-based schemes have also been successfully verified in other transmission systems, such as orthogonal frequency division multiplexing (OFDM), free-space optical (FSO) communication and so on [43]–[47]. In nonlinear photonics, DL methods have been employed to predict ultrafast nonlinear dynamics, generate solitons, and inversely estimate equation parameters [48]–[59]. These advancements suggest DL-based approaches could replace traditional simulation methods, offering low-complexity solutions for waveform-level modeling. However, rigorous validation and critical evaluation of DL-based schemes are essential to ensure their reliability and identify potential limitations, paving the way for future improvements of DL-based schemes in wideband optical fiber transmission.

Accuracy validations for DL-based models commonly employ normalized mean square error (NMSE) as a metrics for waveform errors evaluation. In previous studies, an NMSE threshold of 0.02 is widely regarded as a benchmark for adequate accuracy [29]; however, it may not be adequately in all cases. It is important to note that waveform errors do not directly reflect the quality of transmission (QoT) errors, the relationship between two factors requires further investigation.

In addition, most DL-based schemes are designed for single-channel or few-channel WDM systems operating below 100 GBaud. As transmission rates exceed 150 GBaud and bandwidths expand beyond the traditional C band, the intensification of linear and nonlinear interactions raises questions about the scalability and effectiveness of existing DL methods for next-generation systems.

In this paper, we introduce a DSP-assisted accuracy evaluation method that integrates waveform errors and QoT errors, enabling a detailed evaluation on the accuracy of DL-based schemes. Leveraging advanced linear and nonlinear DSP algorithms, we can analyze the effect of different types of errors on QoT from the perspective of constellations and Q-factor errors aligning with the results of waveform errors, providing a fair and comprehensive accuracy evaluation processing. Furthermore, we review current DL-based waveform modeling schemes, and compare their performance. Results demonstrate that FDD and BiLSTM achieve superior performance among five DL schemes, with a maximal NMSE improvement of 83.1% and a Q-factor error reduction of 1.06 dB in a 5-channel with 50 GBaud configuration. Further tests of FDD in wideband WDM systems with large-channel and high-rate reveal significant performance degradation: NMSE degradation by 92.9%, and Q-factor errors increased by 2.02 dB when scaling from 5 to 25 channels; similarly, NMSE degradation reaches 89.7%, and Q-factor errors rise by 1.33 dB when symbol rates increase from 50 to 200 GBaud. Finally, we analysis the challenges in scaling DL-based waveform-level channel modeling for wideband configurations and propose potential solutions.

The rest of the paper is organized as follow. Section II outlines the architecture of DL-based schemes for WDM systems and discusses their respective advantages. Section III introduces the DSP-assisted accuracy evaluation method. Section IV presents a comparative performance analysis of DL-based schemes using the DSP-assisted accuracy evaluation

method. Section V presents potential solutions to address the challenges in wideband configurations and points out directions for future advancements. Finally, Section VI concludes the paper.

II. OPTICAL FIBER TRANSMISSION SYSTEM

This part introduces the classical coherent optical fiber WDM transmission system, and reviews the SSFM, providing the dataset for following DL models training. The typical coherent WDM transmission simulation system is shown in Fig. 1, including the transmitter, optical fiber channel, and receiver. The parameters of simulation system are detailed in Table I.

At the transmitter side, bit sequences are generated by pseudo-random numbers seed and mapped to symbol sequences using dual-polarized 16 quadrature amplitude modulation (DP-16QAM). The symbol sequences are upsampled by a factor of 4. A root-raised cosine (RRC) filter is used to perform pulse shaping, with a roll-off factor of 0.1. Then, the signals from different channels are modulated onto different frequency carriers to generate WDM signals for fiber transmission. The WDM signals can be expressed as follows:

$$\mathbf{A}(z, t) = \sum_{k=1}^C \mathbf{A}_k(z, t) \exp(j\Delta\omega_k t), \quad (1)$$

where \mathbf{A} represents the optical signals over two arbitrary orthogonal polarization modes \mathbf{A}_x and \mathbf{A}_y . \mathbf{A}_k is the optical signal of k -th channel. z indicates the transmission distance and t represents the time coordinate. C is the total number of WDM channels, and $\Delta\omega_k = \omega_k - \omega_0$ is the difference between the central frequency of k -th channel and the central frequency of WDM signals.

The propagation of optical signal through the single-mode fiber (SMF) is governed by the NLSE, which is expressed as:

$$\frac{\partial \mathbf{A}(z, t)}{\partial z} = (\hat{\mathbf{D}} + \hat{\mathbf{N}})\mathbf{A}, \quad (2)$$

where \mathbf{D} is the linear operator that accounts for the effects of attenuation, chromatic dispersion (CD), and polarization mode dispersion (PMD), and \mathbf{N} is the nonlinear operator that represents the effects of self-phase modulation (SPM), cross-phase modulation (XPM), and four-wave mixing (FWM) related to

TABLE I
PARAMETERS OF SIMULATION SYSTEM

Parameters	Value
Modulation format	DP-16QAM
Roll-off factor of RRC	0.1
Carrier wavelength	1550 nm
Attenuation	0.2 dB/km
Dispersion	17 ps/(nm·km)
Nonlinear coefficient	1.3/(W·km)
Span length	80 km
EDFA noise figure	5 dB

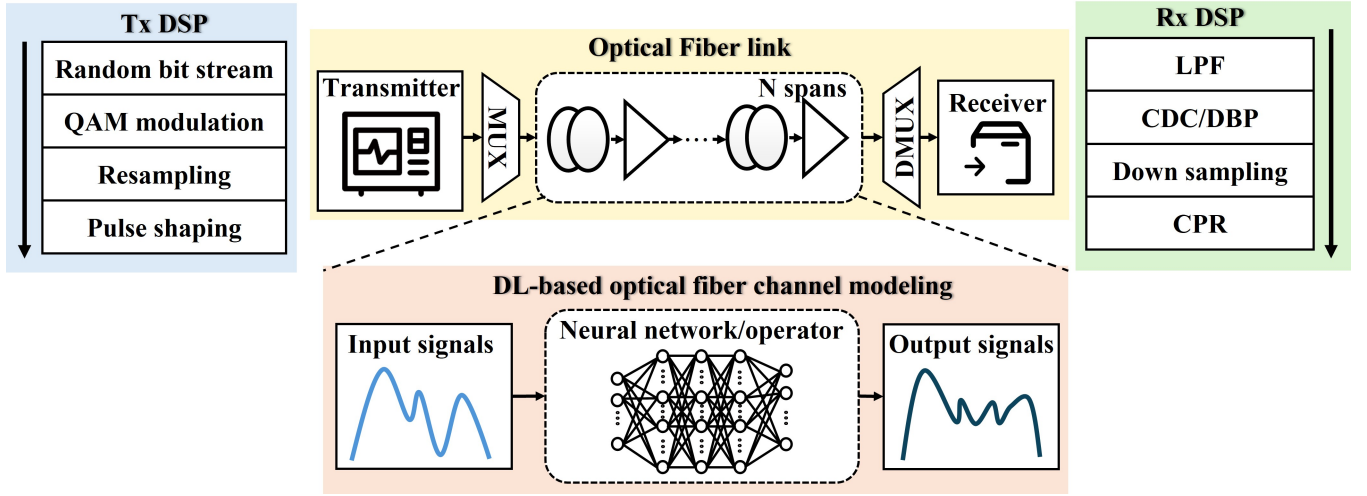


Fig. 1. A coherent simulation system.

the signal energy. When dealing with dual-polarization signals, the NLSE is typically considered in its coupled form, known as the Coupled NLSE (CNLSE) [60], or CNLSE simplified version, the Manakov equation [61], [62]. Here, we employ the Manakov equation to model the fiber channel, which can be expressed as:

$$i \frac{\partial \mathbf{A}}{\partial z} - \frac{1}{2} \beta_2 \frac{\partial^2 \mathbf{A}}{\partial t^2} + \frac{8}{9} \gamma |\mathbf{A}|^2 \mathbf{A} + \frac{\alpha}{2} i \mathbf{A} = -i \frac{\Delta \beta_1}{2} \bar{\sigma} \frac{\partial \mathbf{A}}{\partial t}, \quad (3)$$

where β_2 is the group velocity dispersion parameter, γ is the nonlinear parameter and α is the loss parameter. $\Delta \beta_1$ represents the differential group delay caused by PMD, and σ defines the mode coupling of the two local principal states of polarization (SOP).

The SSFM is the most commonly used numerical method to solve the NLSE. The SSFM divides long-haul optical fiber into numerous small steps, allowing linear and nonlinear operators to be considered independently. The symmetric SSFM operation at each step is expressed as:

$$\begin{aligned} A(z+h, t) \approx & \exp\left(\frac{h}{2} \hat{\mathbf{D}}\right) \exp\left\{h \hat{\mathbf{N}} \left[A\left(z + \frac{h}{2}, t\right)\right]\right\} \\ & \times \exp\left(\frac{h}{2} \hat{\mathbf{D}}\right), \end{aligned} \quad (4)$$

where h is the length in each step. The nonlinear phase rotation method [63], a variable step-size method that is designed for systems dominated by nonlinearity, is employed. According to their characteristic and computational convince, the linear and nonlinear operators are calculated in the frequency and time domain, respectively. At the end of each fiber span, Erbium-doped fiber amplifiers (EDFA) are used to compensate for signal attenuation. However, EDFAs introduce amplified spontaneous emission (ASE) noise, which can be approximated as Gaussian noise.

After transmission through the optical fiber link, receiver-side DSP (Rx DSP) compensates for signal impairments. A matched RRC filter is applied, followed by down-sampling. Chromatic dispersion compensation (CDC) is then performed to address linear impairments. Alternatively, the CDC can be

replaced with the digital backpropagation (DBP) algorithm [64], which compensates for both linear and nonlinear impairments. Subsequently, carrier phase recovery (CPR) and demodulation are executed. Finally, the QoT metrics, such as the Q-factor and GSNR, are evaluated.

The waveforms of full-field WDM signals generated from the SSFM-based simulation system providing a rich dataset for training DL models. Once trained, the DL models can replace the SSFM-based optical fiber channel within the simulation system. The accuracy of the DL models is assessed by comparing their simulation results against those obtained with SSFM.

III. DL-BASED WAVEFORM-LEVEL OPTICAL FIBER CHANNEL MODELING

The primary computational burden in optical fiber transmission simulation arises from the SSFM. Consequently, the DL-based waveform-level schemes basically model the optical fiber channel, using the data generated by SSFM. In the following, we outline the training processing for DL models and provide detailed descriptions of various DL schemes.

A. Training processing

The process of constructing the training dataset involves two main stage: data collection and data preprocessing, as shown in Fig. 2. To mitigate overfitting and reduce pattern prediction by neural networks [], multiple random seeds are employed to generate diverse bit sequences with a NumPy-based random number generator. In this study, ten distinct random seeds are employed. Each generated bit sequence is mapped to a DP-16QAM constellation through the Tx DSP, producing sequences of 7680 symbols, which are transmitted through an SSFM-based optical fiber channel to generate waveform data. The data collection approach depends on the DL scheme, categorized into overall and distributed schemes. In the overall scheme, a single DL model is employed to model the long-distance optical fiber channel, collecting waveform data only at transmission distances of 0 km and X km (the specified transmission distance). Conversely, the distributed

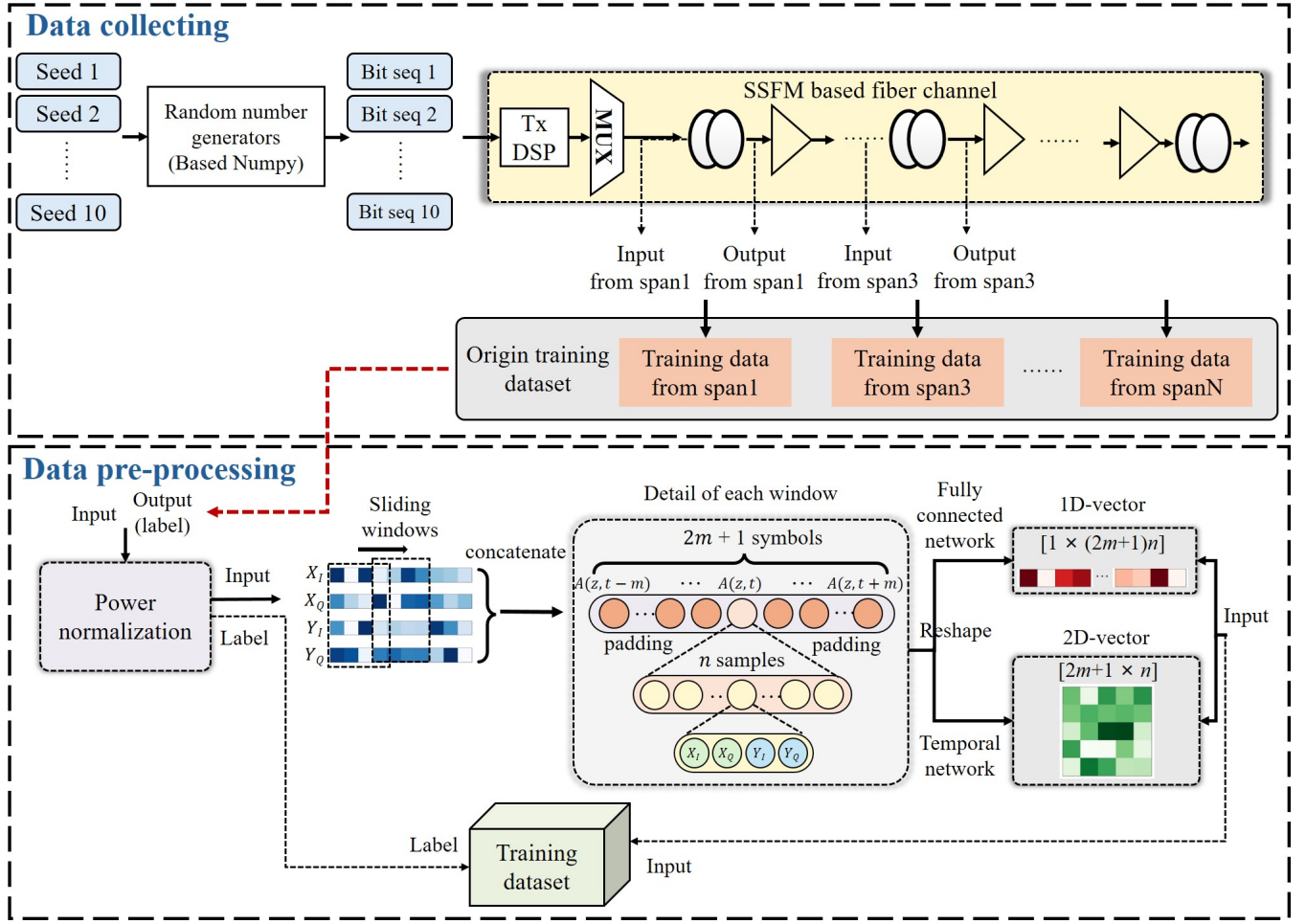


Fig. 2. The specific flow of DSP-assisted accuracy evaluation method.

scheme uses multiple DL models in a cascade, collecting input and output data from multiple 80km fiber spans. This approach enriches the training dataset, enabling the DL model to better adapt to varying transmission characteristics and improving the accuracy of cascaded transmission modeling. Importantly, waveform data is collected at the input and output of each fiber span while excluding the effects of the current span's EDFA. This ensures that only linear and nonlinear effects are captured in the dataset, excluding random noise, as DL models primarily fit deterministic effects, except for generative models such as GANs. In this study, the waveform data is collected from fiber spans [1, 3, 5, 7, 9], forming the origin training dataset.

The next step is to preprocess the origin dataset to accelerate the convergence and adapt it to the specific input requirements of different DL architectures. The preprocessing steps include power normalization, sliding windows, and reshaping. Power normalization is applied to facilitate model convergence by adjusting the input and output signals according to the following equation:

$$\tilde{x} = x \cdot \sqrt{\frac{1}{\sum_{i=1}^{N_{ch}} P_i}}, \quad (5)$$

where N_{ch} represents the total number of the WDM channels, and P_i is the power of the i -th channel. Given that the dataset comprises the complex signals with dual polarization and DL models are better at dealing with real number than complex ones. The complex signals are decomposed into two real-valued components: in-phase (I) and quadrature (Q) signals. At each time step, the real-valued signals of the two polarizations—denoted as X_I , X_Q , Y_I and Y_Q —are concatenated into a one-dimensional vector. To preserve accuracy, it is essential to account for inter-symbol interference (ISI) induced by CD when constructing the input data. The number of symbol affected by ISI is determined using the equation:

$$N_{ISI} = \frac{\Delta T}{\Delta t} = \frac{L\beta_2\Delta\omega}{1/S} = L\beta_2\Delta\omega S, \quad (6)$$

where N_{ISI} represents the number of symbols affected by ISI, ΔT is the temporal width affected by ISI, Δt is the time duration of one symbol, L is the transmission distance, $\Delta\omega$ is the spectrum width, and the S is the symbol rate. To account for ISI, adjacent symbols are included in the input data using a sliding window. The window length is adjusted based on the ISI strength, which varies with the transmission rate, spectrum width, and transmission distance. The input data window consists of symbols at different times, represented

as $[A(z, t - m), \dots, A(z, t), \dots, A(z, t + m)]$, where $A(z, t)$ is a one-dimensional vector aligned at distance z and time t , with dimension d . Here, m is the number of adjacent symbols, typically set as $(N_{\text{ISI}} - 1)/2$, ensuring accurate representation of CD effects. In Chapter 4, the FDD scheme employs a linear decoupling method, enabling the DL model to focus exclusively on fitting nonlinear characteristics. Notably, inter-symbol correlation in residual nonlinearities is shorter than that caused by CD, due to continuous signal power attenuation during fiber propagation. The inter-symbol correlation for nonlinearities can be approximated using the effective nonlinear length, expressed as:

$$\begin{aligned} L_{\text{eff}} &= \frac{1}{\alpha}, \\ N_{\text{NL}} &= L_{\text{eff}} \beta_2 \Delta \omega S, \end{aligned} \quad (7)$$

where L_{eff} presents the nonlinear effective length, and N_{NL} denotes the nonlinear inter-symbols correlations lengths. Each symbol of input window comprises N sample points, with each sample point containing the four-dimensional signals X_I, X_Q, Y_I, Y_Q . Thus, the total dimension d of $A(z, t)$ is calculated as:

$$d = 4N = 4N_{\text{upsample}} N_{\text{ch}} \quad (8)$$

where N_{upsample} is the number of upsampled points for a single-channel SSFM. Typically set to 2 to satisfy the Nyquist sampling theorem, higher values may be employed to enhance SSFM accuracy. In this study, N_{upsample} is set to 4 to balance accuracy and complexity. For WDM transmission, multi-channel signals require multiplexing, and the number of upsampling points is adjusted according to the number of channels to accommodate the expanded spectral range. Following the sliding window processing, the input window is reorganized to meet the specific input requirements of various DL models. For fully connected networks, such as GAN, FNO and DeepONet, input is formatted as a one-dimensional vector containing symbols from $2m+1$ distinct time steps, represented as $[b, (2m+1) * d]$, where b is the batch size. For temporal NNs (such as LSTM and self-attention), the input is structured as a two-dimensional vector, expressed as $[b, 2m+1, d]$, where the second dimension corresponds to different time steps, and the third dimension represents the points within each symbol. Each symbol at a specific time is assigned to the corresponding time location in the LSTM or self-attention unit.

The dataset is divided into training and testing dataset. To evaluate model performance, a distinct random number seed, not present in the training dataset, is used to generate the testing dataset. The loss function employed for training is the smooth L1 (SL1) loss, defined as:

$$\text{smooth}_{L_1}(x) = \begin{cases} 0.5x^2 & \text{if } |x| < 1 \\ |x| - 0.5 & \text{otherwise} \end{cases} \quad (9)$$

SL1 and MSE loss, which is commonly used in previous studies, exhibit no significant differences in final training results. This is because, for most of the training process, the loss remains below 1, resulting in similar gradient values for both loss functions. The number of epochs is set at 1000, with the possibility of increasing for finer accuracy. The Adam optimizer is used with an initial learning rate (LR) of $5E-4$,

with the LR adjusted using a cosine annealing schedule for each parameter group to enhance training accuracy. During testing, sequences are generated using distinct random seeds, ensuring they do not overlap with the training dataset. Identical testing signals are transmitted via both the SSFM and the DL-based optical fiber channels. Waveform error and QoT errors are the primary metrics used to assess the accuracy of DL models, as detailed in Chapter III. Each transmitted sequence consists of 2^{17} symbols per channel, ensuring sufficient length to minimize QoT fluctuations due to overly short sequences.

B. Details of DL-based schemes

Apart from the configuration of the dataset and the training process, another crucial aspect of the DL method is to design a suitable architecture. DL-based schemes leverage deep neural networks to learn hidden correlations and patterns from large datasets, bypassing the need for complex prior mathematical and physical knowledge. With the advent of advanced hardware like the graphics processing unit (GPU), computational time is significantly reduced through parallel processing. In the following, we make a comprehensive review of structures and advantages of various DL models.

We divide the DL schemes into several categories, shown in Table II. The transmission mode, which pertains to the use of single or multiple models for achieving long-haul transmission; driven mode, which assesses whether physical principles combining with the DL models; and network structure, which relates to the specific parameterized architecture employing. The specific classification is as follows:

- Transmission mode: overall or distributed.
- Driven mode: pure-data driven or data-physics hybrid-driven.
- Network structure: neural network or neural operator

These classifications aids in a clearer understanding of the various DL-based approaches, providing a comprehensive framework for analyzing their effectiveness and applicability.

1) *Overall schemes and distributed schemes*: Optical fiber links typically consist of several components: optical fibers, optical amplifiers, wavelength selective switches (WSS), variable optical attenuator (VOA), optical couplers and so on. Optical transmission links over long distances consist of a cascade of multiple optical fibers and optical amplifiers. For achieving long-haul optical link modelling, DL-based schemes utilize two main ways: overall schemes and distributed schemes, which means using single or multiple models to achieve long-haul transmission.

Overall schemes treat the entire fiber link as an integrated module and use single network to model the entire fiber link. These approaches are exemplified by the overall BiLSTM [29] and overall CGAN [30]. The overall BiLSTM scheme is the first DL-based optical fiber channel modeling scheme in optical transmission and has demonstrated high accuracy in intensity modulation and direct detection (IMDD) systems for distances ranging from 10 to 80 km. However, it is limited to short distance transmission due to deterministic nature of BiLSTM, which cannot effectively fit random noise between each fiber span. To extend to long-haul transmissions, the

TABLE II
EXISTING DL-BASE WAVEFORM-LEVEL OPTICAL FIBER CHANNEL MODELING SCHEMES

Schemes	Transmission mode	Driving mode	Network structure	Channel number	Symbol rate (GBaud)	Modulation format	Distance (km)	Reference
BiLSTM	△	□	◇	1	10	PAM4	80	[29]
CGAN	△	□	◇	1	30	16QAM	1000	[30]
FNO	▲	□	◆	1	28	64QAM	1200	[31], [32]
Multi-head attention	▲	□	◇	1	40	16QAM	1000	[33]
Co-LSTM	▲	□	◇	1	32	DP-16QAM	2800	[34]
PINO	▲	■	◆	1	14	16QAM	320	[35]
DNN	▲	□	◇	2	30	16QAM	80	[36]
FNO	▲	□	◆	5	30	DP-16QAM	800	[37]
FDD	▲	■	◇	41	30	DP-128QAM	1040	[38], [39]
DeepONet	▲	□	◆	96	100	DP-16QAM	800	[41], [42]

¹ Overall: △ Distributed: ▲ Pure data-driven: □ Data-physics hybrid-driven: ■ Neural network: ◇ Neural operator: ◆

CGAN scheme was introduced. CGAN, a generative model, can fit specific distributions to address the challenge of random noise fitting. It has achieved fast and accurate fiber channel modeling up to 1000 km in a coherent transmission system. However, its adversarial training approach is not easy to converge to the best performance [65], particularly limits its application in multi-channel WDM systems.

Distributed schemes were developed to enhance the capabilities of DL-based schemes by mimicking the actual structure of long-haul optical fiber links. In distributed schemes, the entire optical fiber link is treated as multiple modules rather than a single integrated module, and each DL model is only responsible for modeling one span fiber and flexibly handle the random noise between each span. Related studies utilized this structure include FNO, self-attention mechanisms, Co-LSTM, PINO, FCNN, FDD, and DPON schemes [31]–[39], [41], [42]. In these works, each model employs the same or slightly fine-tuned parameters to model the response of a single fiber span and multiple models are cascaded to achieve long-haul transmission. Distributed schemes have shown robust performance in both single- and multi-channel WDM systems. By focusing on the characteristics within a single fiber span, these schemes avoid the complexities of modeling the entire fiber link, including linear and nonlinear effects that accumulate with distance, as well as the amplifier noise, which is challenging for deterministic DL models. These specificities simplify the features that the DL models need to learn, facilitating faster convergence and improved accuracy. Additionally, distributed schemes allow for flexible adjustments in transmission length by varying the number of cascaded models. However, the iterative cascading of multiple models introduces inevitable iterative errors that degrade performance under long-haul transmission. Some researches address these iterative errors by constructing multi-span datasets for training DL models [39] or by fine-tuning the models used in later spans [33], [34], [42]. Despite challenges of iterative errors, distributed schemes offer higher accuracy and flexibility compared to overall schemes, making them potential mainstream methods for wideband and

long-haul optical transmission systems.

2) *Pure data-driven schemes and data-physics hybrid-driven schemes*: DL-based schemes directly learn the entire mapping relationship between input and output signals collected from the SSFM-based simulation and don't need any prior physical knowledge, which is called pure data-driven schemes. To enhance the accuracy, some studies incorporate prior physical knowledge, which is called data-physics hybrid-driven schemes.

Pure data-driven schemes rely solely on data collected from the SSFM-based simulation, including pairs of channel input and output waveforms. During training, loss functions such as mean squared error (MSE) or SL1 loss are utilized to optimize the model, making it converge to the features of the training data. These schemes are favored for their simplicity, involving training data collection, dataset construction, and neural network training. However, the challenge lies in accounting for all characteristics, including complex linear and nonlinear impairments within the optical fiber channel. This can complicate the training process, and loss functions that only reflect waveform errors may lead to suboptimal solutions that do not satisfy the NLSE properties.

To enhance the accuracy of pure-data driven methods, data-physics hybrid-driven schemes were proposed to integrate physical principles into the training process. The FDD scheme separates optical channel characteristics into linear and nonlinear components. Physical models are employed for modeling linearity, and neural networks are utilized for modeling nonlinearity. FDD ensures highly accurate linearity modeling while reducing the complexity of neural network fitting features and improving the accuracy of nonlinearity modeling. The PINO scheme represents another innovative data-physics hybrid-driven approach, utilizing DeepONet for channel modeling with the NLSE integrated into the loss function. This allows for unsupervised training, significantly reducing both the amount of training data required and the complexity of training. Compared to pure-data driven method, such as BiLSTM, the PINO and FDD have demonstrated higher accuracy and lower complexity in single-channel

and multi-channel WDM systems. Additionally, hybrid models help in circumventing the uncertainty inherent in pure-data driven models and address the overfitting problem often encountered with training datasets.

3) *Neural network schemes and neural operator schemes:* DL-based schemes relying on neural networks have exhibited outstanding outcomes in the aspect of optical fiber channel modeling. In recent years, the deep neural operator, as a novel deep learning approach, has been developed rapidly and demonstrated a strong generalization capability as a solver for PDEs.

Neural networks, underpinned by the universal approximation theorem, can approximate any continuous function with arbitrary precision given sufficient network depth and complexity. They learn mappings between discrete vector spaces. Various neural networks, such as CGAN, BiLSTM, and Transformer have demonstrated high accuracy in optical fiber channel modeling. CGAN consists two parts: generator and discriminator represented by FCNN. Through adversarial training, generator mimics data distributions to fool the discriminator. However, it struggles with convergence in complex multi-channel WDM systems. BiLSTM, a typical variant of RNN network, can capture temporal correlations characteristics through its forward and backward recurrent structure. It has been successfully applied in both single-channel IMDD systems and WDM coherent systems. Transformer leverages a self-attention mechanism, offering parallel computation capabilities and overcoming the long-term memory issues typical of RNNs.

Neural operators represent a paradigm shift by learning mappings between infinite-dimensional function spaces, a more generalized approach compared to discrete vector spaces typically handled by neural networks. Two typical neural operators, FNO and DeepONet, have been introduced in optical fiber channel modeling. FNO utilizes Fourier transform techniques to create new solution maps for the NLSE from both time-domain and frequency-domain perspectives in single-channel and multi-channel WDM systems. DeepONet, consisting of branch and trunk networks, excels at capturing the intricate relationships between input and output functions. This operator can incorporate the NLSE into its loss functions to enhance model convergence by embedding physical constraints, as the input of the trunk network includes distance and time coordinates, which can be differentiated automatically. Through a stacked-DeepONet architecture, it can be successfully applied to a fully-loaded C+L-band WDM system. The advantages of neural operator are stronger generalization. As the goal of neural operators is learning is to approximate the mapping between function spaces, and once this mapping is learned, the parameterized operator can consistently locate the correct solution in the objective function space, regardless of changes in initial conditions. This generalization ability has proven effective for varying launch power in optical fiber channel modeling.

Overall, neural networks with efficient structural designs and neural operators with stronger generalization have demonstrated distinct advantages in optical fiber channel modeling. Further research is warranted to explore how to tightly inte-

grate the strengths of both for enhanced application in this field.

IV. THE ACCURACY EVALUATION METHOD FOR DL-BASED SCHEMES

DL-based optical fiber channel modeling aims to uncover hidden correlations and patterns from datasets generated by SSFM-based simulation. Accuracy evaluation plays a crucial role in determining whether DL-based schemes can serve as reliable alternatives to SSFM. This section reviews existing accuracy evaluation metrics and discusses their potential limitations. Furthermore, we propose a DSP-assisted accuracy evaluation method to overcome these shortcomings in existing metrics, offering a fair and comprehensive approach for assessing accuracy and establishing a robust foundation for comparing various DL-based schemes in wideband WDM systems.

A. The metrics for accuracy evaluation

Accuracy metrics for DL-based optical fiber channel waveform modeling typically include waveform errors and QoT errors, serving to assess whether DL-based schemes accurately replicate the performance of the SSFM. Waveform errors are analyzed by comparing deviations in the waveform profiles and quantitatively measured using the NMSE, defined as:

$$NMSE = \frac{\sum_{i=1}^{N_{data}} |\hat{y}_i - y_i|^2}{\sum_{i=1}^{N_{data}} |y_i|^2}, \quad (10)$$

where N_{data} is the number of the data size, y and \hat{y} denote the outputs from SSFM and DL-based schemes, respectively. When ASE noise from the EDFA incorporated, the same random noise is applied to both SSFM and DL-based schemes during NMSE calculations to ensure that identical consistency and avoid significant discrepancies in NMSE values. Previous studies have established an NMSE threshold of less than 0.02 as indicative of sufficiently accurate DL models [29].

In addition to waveform errors, QoT errors serve as crucial metrics for evaluating the practical reliability of DL-based schemes in applications, such as DSP algorithm design and system parameter optimization. To evaluate the QoT errors, compensation for channel impairments is necessary through advanced DSP algorithms. Constellations are commonly used for communication signal performance analysis, offering an intuitive visualization of noise distribution by examining the positions of constellation points. After CPR, the GSNR is calculated to quantify the noise level of received signals. GSNR is defined as:

$$GSNR = 10 \log_{10} \left(\frac{P_s}{\mathbb{E}[rx - tx]^2} \right) = 10 \log_{10} \left(\frac{P_s}{P_{ASE} + P_{NL}} \right), \quad (11)$$

where rx and tx are the received and transmitted samples, respectively, P_s is the signal power, P_{ASE} is the ASE noise from the EDFA, and P_{NL} denotes the nonlinear noise introduced by optical fibers. Subsequently, demodulation is performed to calculate the bit error rate (BER) and Q-factor, defined as:

$$BER = \frac{N_{error}}{N_{bits}} \quad (12)$$

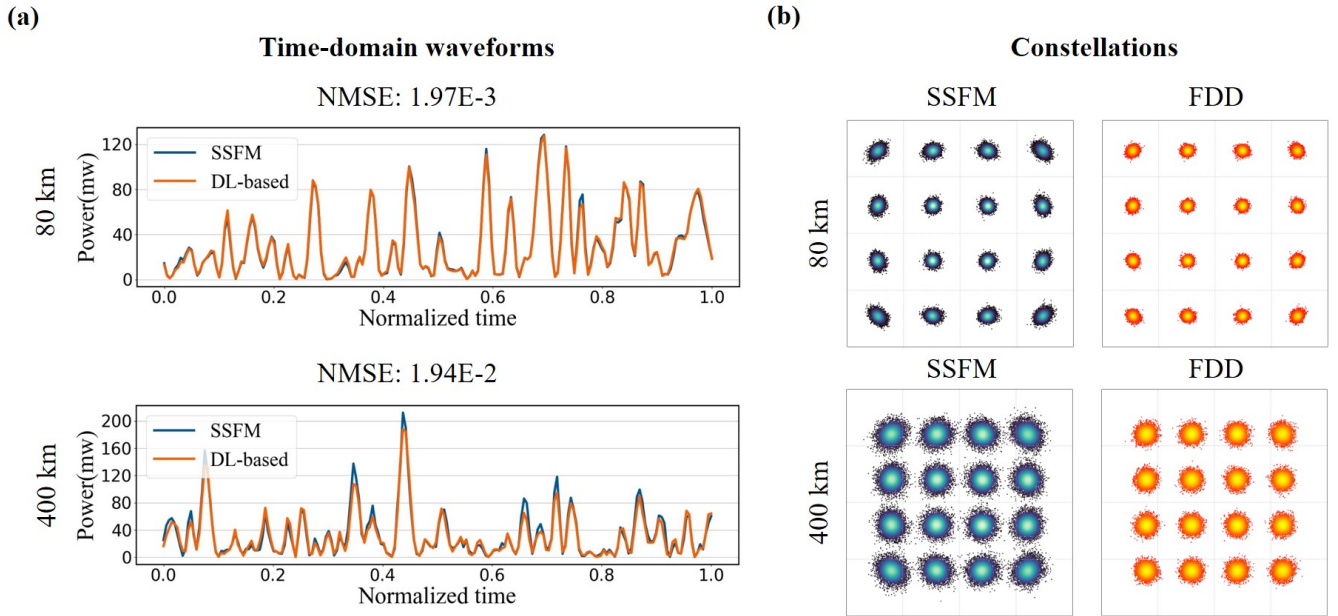


Fig. 3. Comparison of DL-based scheme and SSFM at 80 km and 400 km. (a) Time-domain waveforms and NMSE values. (b) Constellations after linear DSP.

$$Q = 20 \log_{10} \left(\sqrt{2} \operatorname{erfc}^{-1}(2BER) \right), \quad (13)$$

where N_{error} is the number of erroneous bits, N_{bits} is the total number of bits, and $\operatorname{erfc}(x)$ is complementary error function. The Q-factor is a logarithmic transformation of the BER, implies that identical Q-factor errors correspond to varying error levels at different BER values. To ensure fair comparisons under varying BER conditions caused by nonlinear and random noise accumulation across different transmission distances or WDM configurations, the Q-factor is consistently evaluated at a fixed BER level by introducing additional random noise at the receiver side. This noise, applied to the received signals for both SSFM and DL-based schemes, is generated using same random seed. In this study, the BER is maintained at the forward error correction (FEC) threshold of $4E-2$ for Q-factor calculations.

B. The potential limitations of accuracy metrics

The previously discussed metrics are widely employed to evaluate the accuracy of DL-based optical fiber channel waveform modeling, offering valuable insights into the performance differences between DL-based methods and SSFM. However, the interrelationship between these metrics remains inadequately explored. Notably, it is unclear whether the acceptable NMSE threshold should vary across different scenarios, or if reductions in waveform errors directly correspond to improvements in QoT errors. In the following, we investigate these questions and provide illustrative examples to clarify these relationships.

1) *The acceptable NMSE threshold:* An NMSE threshold of 0.02 has been established as acceptable benchmark for DL-based schemes in previous studies and widely adopted in subsequent research [29], [30], [38]. However, its applicability to scenarios involving strong nonlinearities, multi-channel

configurations, and high launch power remains insufficiently validated.

To evaluate the suitability of this threshold under strong nonlinear conditions, we analyze the performance of FDD schemes in an 11-channel configuration with a transmission rate of 140 GBaud and a launch power of 8 dBm—approximately 4 dBm higher than the optimal launch power. First, waveform errors are assessed by examining the time-domain waveforms and NMSE values between FDD and SSFM. Fig. 3(a) shows the time-domain waveforms and their NMSE at both 80 km and 400 km transmission, with NMSE values of $1.97E-3$ and $1.94E-2$, respectively—both below the accepted threshold of 0.02. Next, we assess noise distribution for both FDD and SSFM to explore the relationship between the acceptable NMSE threshold and QoT errors. Fig. 3(b) displays the constellations of FDD and SSFM after linear DSP at 80 km and 400 km. The constellations of FDD exhibit less noise accumulation than SSFM, particularly regarding nonlinear phase rotation associated with signal power. These results highlight that even when waveform distortions fall within the acceptable NMSE threshold, noise distribution discrepancies can be significant. The primary reason for this disparity is the treatment of nonlinearity as a perturbation term [66], which minimally affects waveform distortions but significantly influences noise accumulation and QoT. Accurate modeling of random and nonlinear noise is essential, particularly for applications such as nonlinear compensation algorithm optimization and E2E system design. These findings indicate that the NMSE threshold of 0.02 is insufficient in scenarios with strong nonlinearities. Defining a universal NMSE threshold across varying scenarios remains challenges. Nevertheless, NMSE continues to serve as a valuable relative metric for evaluating the accuracy of DL models, with lower NMSE values indicating better performance. Notably, further

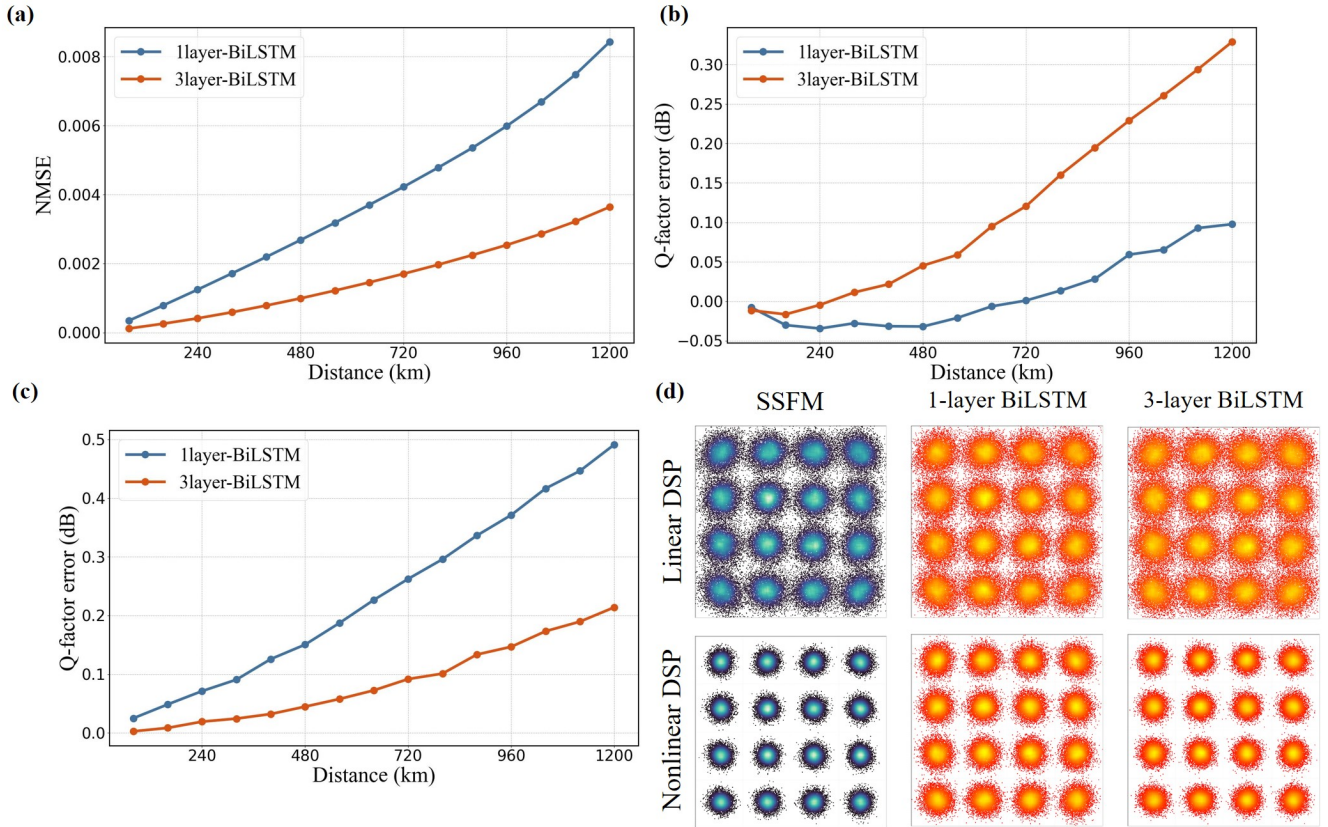


Fig. 4. Comparison of 1-layer and 3-layer BiLSTM between SSFM. (a) NMSE curve covering 1200 km. (b) Q-factor error after linear DSP processing covering 1200 km. (c) SNR error after nonlinear DSP processing covering 1200 km. (d) Constellations after linear and nonlinear DSP processing at 1200 km.

accuracy evaluation should incorporate complementary QoT error analyses for a more comprehensive assessment.

2) *The fluctuation of QoT for distributed schemes:* Waveform errors alone are insufficiently for evaluating the accuracy of nonlinear modeling, due to their perturbative nature. To gain a more comprehensive understanding of the accuracy of DL models, deeper analysis of QoT errors is necessary. Metrics such as GSNR and Q-factor are commonly used for QoT error analysis. However, in distributed schemes, the calculation of QoT errors is influenced by factors, such as nonlinear modeling errors and iterative errors, that lead to anomalous fluctuations, causing inconsistencies between waveform errors and QoT errors, thereby complicating the assessment of model accuracy. This phenomenon termed “anomalous QoT fluctuations,” is explored in detail in this section.

To investigate the alignment between waveform and QoT errors, we conduct test using FDD schemes in a 3-channel WDM system with a transmission rate of 50 GBaud and a launch power of 4 dBm—approximately 4 dBm higher than the optimal launch power. To adjust the accuracy of FDD, we vary the number of BiLSTM layers used for nonlinear modeling, comparing configurations with 1 and 3 layers. Both models are trained on the same dataset with identical training hyperparameters. First, waveform errors are evaluated using NMSE. Fig. 4(a) shows the NMSE curves over a 1200 km transmission range for both 1-layer and 3-layer BiLSTM models. The 3-layer BiLSTM achieves consistently lower NMSE values

than the 1-layer BiLSTM, demonstrating superior waveform modeling due to its deeper network and enhanced ability to capture nonlinearities. Next, QoT errors are assessed using the Q-factor, calculated by subtracting the Q-factor of the DL models from those of SSFM. Fig. 4(b) shows that Q-factor errors for the 1-layer BiLSTM remain below 0.1 dB over the 1200 km transmission range, whereas Q-factor errors for the 3-layer BiLSTM increase with distance, peaking at 0.33 dB. These results suggest that the 1-layer BiLSTM model more closely matches the QoT of SSFM. Surprisingly, these results suggest that the 1-layer BiLSTM more closely matches the QoT of SSFM, despite the 3-layer BiLSTM achieving better NMSE performance. This inconsistency complicates the task of determining which model is truly more accurate.

The inconsistency between waveform and QoT errors arises from two key factors: channel effect fitting errors and iterative errors. In FDD schemes, linear effects are modeled using physical models, while DL models handle nonlinear effects, so the channel effect fitting errors mainly refers to the nonlinear fitting errors. Nonlinear fitting errors occur when the DL model’s representation of nonlinearities is less accurate than SSFM, resulting in a lower nonlinear noise levels in the DL model. This leads to higher Q-factors for DL models compared to SSFM, producing negative Q-factor errors ($Q_{\text{SSFM}} - Q_{\text{DL}} < 0$). The second factor is iterative errors, which occur in distributed schemes due to the cascading of multiple DL models for long-haul transmission. Errors from earlier models propagate to

subsequent ones, leading to error accumulation over the transmission path. Iterative errors degrade the QoT of DL models, resulting in positive Q-factor errors ($Q_{\text{SSFM}} - Q_{\text{DL}} > 0$). Over long distances, nonlinear fitting errors tend to drive Q-factor errors into the negative region, while iterative errors push them positive. The interplay between these two factors causes the "anomalous QoT fluctuations" phenomenon, explaining the observed inconsistencies between waveform and QoT errors, particularly over extended transmission distances.

To further understand "anomalous fluctuations of QoT", we compare the results for the 1-layer and 3-layer BiLSTM models. Fig. 4(b) shows that, at short transmission distances, Q-factor errors for the 1-layer BiLSTM are negative, indicating dominance of nonlinear fitting errors. At these distances, iterative errors are minimal due to limited error accumulation. As transmission distance increases, iterative errors begin to dominate, degrading the Q-factor of the 1-layer BiLSTM and shifting Q-factor errors into the positive region. At 1200 km, the combined effect of nonlinear fitting and iterative errors results in a Q-factor error of only 0.1 dB for the 1-layer BiLSTM. In contrast, Q-factor errors for the 3-layer BiLSTM remain positive throughout the transmission range, except for the initial spans. The higher accuracy of the 3-layer BiLSTM in nonlinear fitting reduces nonlinear fitting errors, allowing iterative errors to dominate across the entire transmission range. Consequently, Q-factor errors for the 3-layer BiLSTM increase with distance. These findings reveal that lower Q-factor errors do not necessarily indicate superior accuracy, as they may result from a fortuitous cancellation of nonlinear fitting and iterative errors.

3) *DSP-assisted accuracy evaluation method*: To ensure a fair and robust comparison of various DL models, a comprehensive accuracy evaluation method is essential. Challenges such as the difficulty in defining a universally accepted NMSE threshold and the phenomenon of "anomalous QoT fluctuations" complicate the assessment process. The inconsistency between waveform and QoT error results further underscores the inadequacy of relying solely on a single metric, such as NMSE or QoT, for evaluating DL approaches. To address these challenges and establish a reliable benchmark for comparing DL models, we propose a DSP-assisted accuracy evaluation method. This approach incorporates multiple metrics, including waveform and QoT errors, and leverages advanced DSP algorithms to compensate for channel impairments such as linear and nonlinear effects. By eliminating QoT fluctuations caused by the coupling of nonlinear modeling and iteration errors, this method provides consistent and reliable results. The DSP-assisted evaluation consists of two key steps: waveform error analysis and QoT error analysis, as illustrated in Fig. 5.

In the first step, NMSE is calculated for filtered single-channel signals. Full-field multi-channel WDM signals from both SSFM-based and DL-based optical fiber links are demultiplexed to extract filtered single-channel signals. Since waveform errors directly correspond to the loss function during DL model training, NMSE serves as an effective and relative metric for assessing DL model accuracy. Lower NMSE values indicate greater accuracy in waveform modeling.

The second step involves evaluating QoT errors, focusing

on the accuracy of channel effect modeling, particularly nonlinear effects. Assessing QoT for DL-modeled signals after linear DSP is challenging due to anomalous QoT fluctuations caused by nonlinear modeling and iteration errors. These errors influence QoT in opposite directions and may cancel each other out over long-haul transmissions, leading to unreliable QoT results. To address this issue, we propose incorporating a nonlinear compensation algorithm—multi-channel DBP—as part of the DSP-assisted accuracy evaluation method. This algorithm compensates for both linear and nonlinear impairments by inversely solving the NLSE. Unlike traditional single-channel DBP, multi-channel DBP operates on full-field multi-channel WDM signals, enabling joint compensation of intra-channel and inter-channel nonlinearities. Key parameters for the multi-channel DBP algorithm include the nonlinear coefficient γ and the step size configuration for each span. In this study, the parameters are set to match those of SSFM exactly: γ is set to 1.137 and the step size configuration using the maximum phase rotation method, with the maximum phase rotation of 0.005. This configuration ensures that the multi-channel DBP algorithm mirrors the inverse process of SSFM. For SSFM, multi-channel DBP compensates nearly perfectly for both linear and nonlinear impairments. However, for DL schemes, the underfitting of nonlinear effects leads to "compensation overflow," where additional nonlinear impairments are introduced. This transforms nonlinear modeling errors into extra nonlinear distortions, aligning their impact with that of iteration errors and mitigating anomalous QoT fluctuations.

QoT error analysis is performed using both linear and nonlinear DSP algorithms applied to filtered single-channel signals. Linear DSP, applied after single-span transmission, isolates the impact of nonlinear modeling errors by eliminating iteration errors. Nonlinear DSP, applied after multi-span transmission, evaluates cumulative nonlinearities without interference from iteration errors. Qualitative assessments involve comparing constellations at various transmission stages. Constellations after linear DSP reveal the DL model's ability to capture nonlinearities, particularly nonlinear phase rotation. Constellations after nonlinear DSP reflect the accuracy of cumulative nonlinearity modeling. Quantitative assessments use metrics such as GSNR, BER, and Q-factor to compare QoT errors and determine the feasibility of using DL models as replacements for SSFM in practical applications.

To validate the effectiveness of the multi-channel DBP algorithm, we apply it to SSFM, 1-layer BiLSTM, and 3-layer BiLSTM models and compare the results. Fig. 4(d) shows constellations after both linear and nonlinear DSP at an 800 km transmission distance. After linear DSP, constellations for both BiLSTM models closely resemble SSFM, making them difficult to distinguish. However, after nonlinear DSP, the 3-layer BiLSTM constellations closely align with SSFM, while the 1-layer BiLSTM exhibits significant deviations and pronounced nonlinear distortions. These observations validate that the multi-channel DBP algorithm effectively transforms channel effects fitting errors into additional distortions. Further validation is provided by analyzing Q-factor errors. Fig. 4(c) illustrates Q-factor errors over a 1200 km transmission range. The 1-layer BiLSTM exhibits higher Q-factor errors, peaking

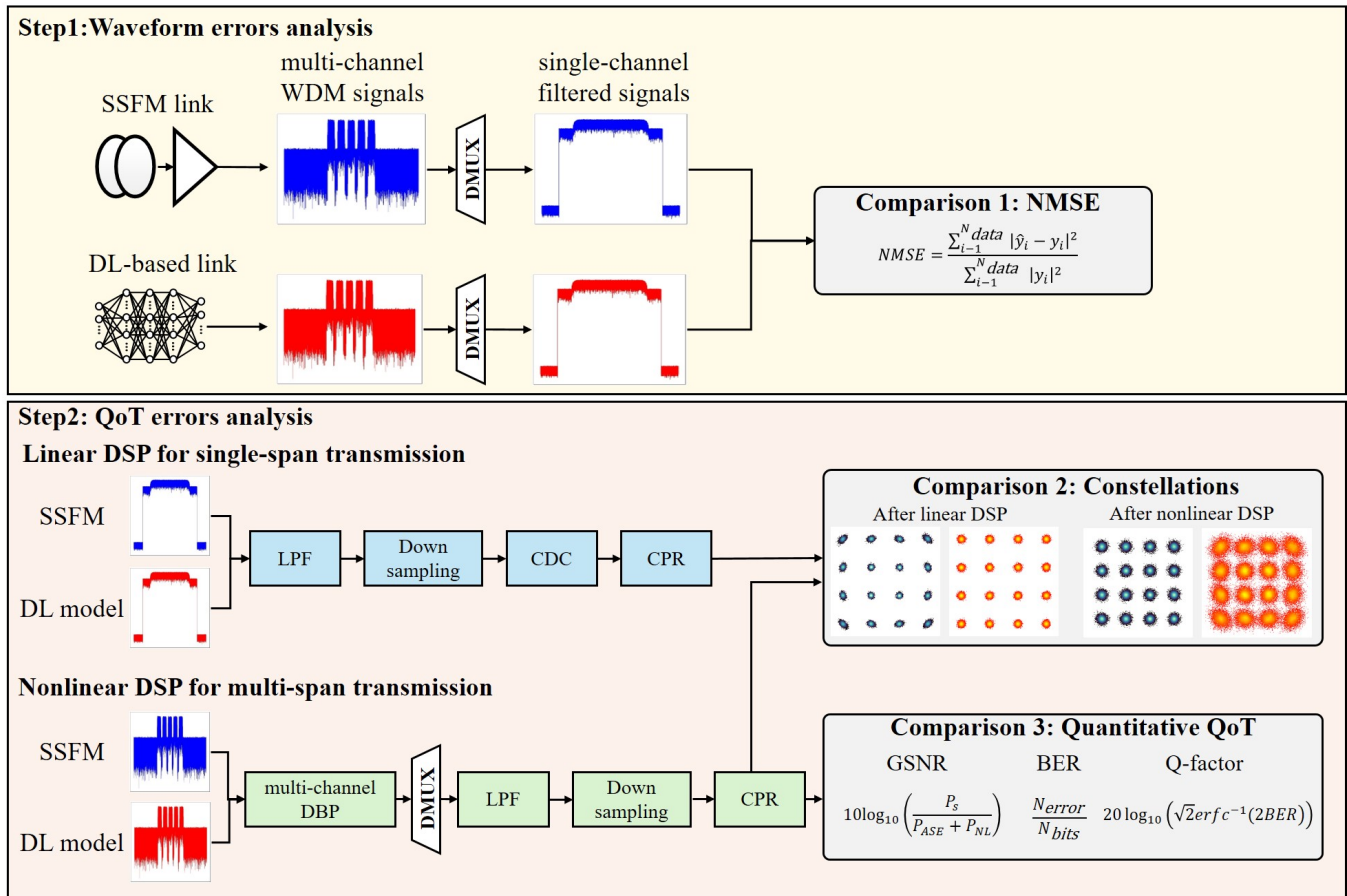


Fig. 5. The specific flow of DSP-assisted accuracy evaluation method.

at 0.5 dB, compared to the 3-layer BiLSTM, which has a maximum error of 0.21 dB. These results indicate that the 3-layer BiLSTM more accurately mirrors the nonlinearity of SSFM. The alignment of Q-factor error results with NMSE further demonstrates that the multi-channel DBP algorithm effectively integrates waveform and QoT error analyses at long-haul transmission. By mitigating anomalous QoT fluctuations, the DPS-assisted accuracy evaluation method provides a fair and reliable approach for assessing DL model accuracy.

In summary, we propose a DSP-assisted accuracy evaluation method that integrates multiple metrics, including waveform and QoT errors, to provide a fair and comprehensive assessment of DL model accuracy. This method establishes a robust and equitable benchmark for comparing various DL models, as discussed in the next section.

V. COMPARISON OF DL-BASED SCHEMES

DL-based optical fiber channel modeling schemes have demonstrated comparable accuracy with significantly reduced complexity relative to traditional SSFM, highlighting their potential as efficient tools for fast and accurate fiber channel simulation. Currently, DL methods are primarily applied to single-channel and few-channel WDM systems, or simplified wideband WDM configurations, with their performance in wideband scenarios remaining inadequately explored. Moreover, existing DL approaches lack a fair and comprehensive

comparison under unified conditions and standards. Such comparative analysis is vital for refining DL models and driving their evolution towards wideband WDM systems. In this section, we first conduct a fair and comprehensive comparison of the existing DL schemes within a few-channel WDM system employing our proposed DSP-assisted accuracy evaluation method. Following this, we extend the best-performing model from few-channel systems to wideband configurations with more WDM channels and higher transmission rates to evaluate the robustness and reliability of DL models in more complex scenarios.

A. Comparisons in few-channel and low-rate WDM systems

DL-based schemes have demonstrated outstanding performance in few-channel WDM system, motivating a comparative evaluation in a 5-channel WDM configuration. The transmission rate is set at 50 GBaud, with a launch power of 4 dB per channel, creating a highly nonlinear scenario that demands robust model performance. To provide a thorough comparison of existing DL-based approaches, the evaluation is divided into two parts: the first evaluates overall versus distributed methods, while the second contrasts pure-data driven approaches with data-physics hybrid-driven methods, also including both neural networks and neural operators. This comparative framework offers a more comprehensive understand of different types of frameworks, beyond focusing on specific schemes.

TABLE III
THE PARAMETERS OF DL MODELS FOR COMPARISON BETWEEN OVERALL AND DISTRIBUTED SCHEMES.

	CGAN			Overall-BiLSTM	Distributed-BiLSTM
	Generator	Discriminator			
Input size	13200	2	Input size	80	80
Hidden layer	4	4	Layers	3	3
Hidden size	[52600,6575,3287,1643,80]	[52640,6580,3290,1645,1]	Hidden size	80	80
Output size	80	20	Time steps	657	165

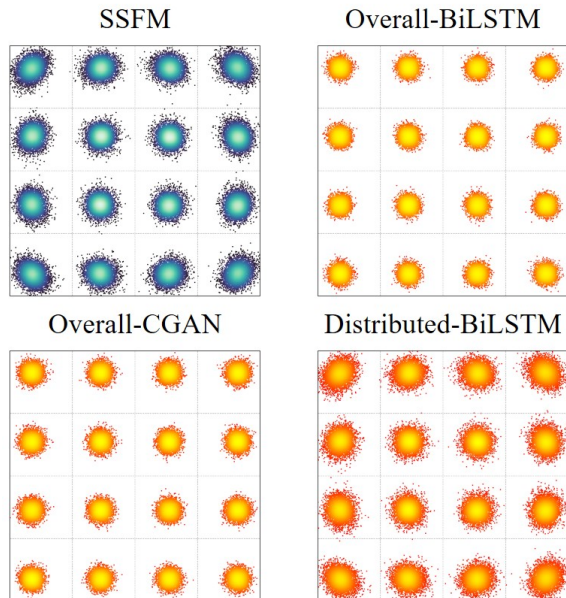


Fig. 6. Constellations of SSFM, overall-BiLSTM, overall-CGAN and distributed-BiLSTM at 320 km transmission.

TABLE IV
PERFORMANCE COMPARISON OF OVERALL AND DISTRIBUTED SCHEMES AT 800 KM TRANSMISSION.

Scheme	NMSE	Q-factor error(dB)
Overall-BiLSTM	0.0133	0.53
Overall-CGAN	0.0151	0.67
Distributed-BiLSTM	0.0011	0.16

1) *Overall schemes vs. distributed schemes:* We compare the performance of both overall and distributed schemes. Specifically, the models compared include overall-BiLSTM, overall-CGAN, and distributed-BiLSTM. Network parameters are meticulously tuned to ensure optimal performance in WDM systems. The overall schemes utilize a single network to model the entire 320 km fiber link, whereas the distributed schemes employ four networks with identical parameters to model the cascaded transmission over the same distance. To address the ISI effects due to CD accumulated over distances, the window length for distributed schemes is set at 211, while for overall schemes, it is 4 times of distributed schemes and extended to 844. The performance of these models is

assessed using the DSP-assisted method described in Section III, ensuring a comprehensive evaluation that accounts for waveform errors and QoT.

To demonstrate the superior accuracy of distributed schemes over overall schemes, we first examine their waveform modeling capabilities. The NMSE for each scheme at a transmission distance of 320 km is presented in Table IV. Here, the NMSE is 0.0133 for overall-BiLSTM and 0.0151 for overall-CGAN, whereas the distributed-BiLSTM achieves a significantly lower NMSE of 0.0011. This indicates a more precise waveform modeling capability by the distributed schemes.

Further analysis of QoT is conducted by examining the constellations after linear DSP processing, shown in Fig. 6. The shapes of the constellations from overall schemes are dissimilar to that of SSFM, suggesting their inability to adequately represent both the random and nonlinear noise characteristics of the fiber link. Additionally, the Q-factor error after nonlinear DSP for overall-BiLSTM is 0.53 dB and 0.67 dB for overall-CGAN, whereas the distributed-BiLSTM is only 0.16 dB, indicating a QoT gap between overall schemes and SSFM.

Notably, the overall-BiLSTM utilizes deterministic fitting models, which are inherently limited in handling random noise. This limitation makes overall schemes with deterministic models particularly unsuitable for long-haul fiber links. The overall-GAN, a generative model, can learn random distributions, but achieving convergence in multi-channel WDM systems is challenging, as the adversarial training mode [67]. In contrast, distributed schemes, which individually model the channel effects of each span, simplifying the linear and nonlinear effects accumulated with the transmission distance and provide a more efficient approach. Meanwhile, they can directly model the random noise between spans using known distributions, thus reducing the influence of random noise. Therefore, distributed schemes are highly suitable for long-distance, multi-channel WDM systems and represents the main technical approach for future wideband WDM systems.

2) *Pure data-driven schemes vs. data-physic hybrid-driven schemes:* Distributed schemes offer notable advantages in accuracy and flexibility, making them the preferred design in recent DL-based optical fiber channel modeling approaches. Accordingly, all methods compared here are implemented as distributed schemes. This section contrasts pure data-driven methods and data-physics hybrid-driven methods, encompassing both neural networks and neural operators. The pure data-driven schemes include BiLSTM [29], Multi-head Attention

TABLE V
THE PARAMETERS OF DL MODELS FOR COMPARISON BETWEEN PURE DATA-DRIVEN AND DATA-PHYSIC HYBRID-DRIVEN SCHEMES.

	DeepONet		FNO	
	Branch Net	Trunk Net		
Input size	13200	2	Input size	13200×1
Hidden layer	4	4	Fourier layer	4
Hidden size	[6600,3300,1650,825,412]	[256,256,256,256,256]	Hidden dimension	16
Output size	80	20	Fourier mode	6600
	BiLSTM	FDD-BiLSTM	Multi-head Attention	
Input size	80	80	Input size	80
Hidden size	80	80	Hidden size/FNN size	80/320
Layers	3	3	Layers	3
Time step	165	45	Time step	165

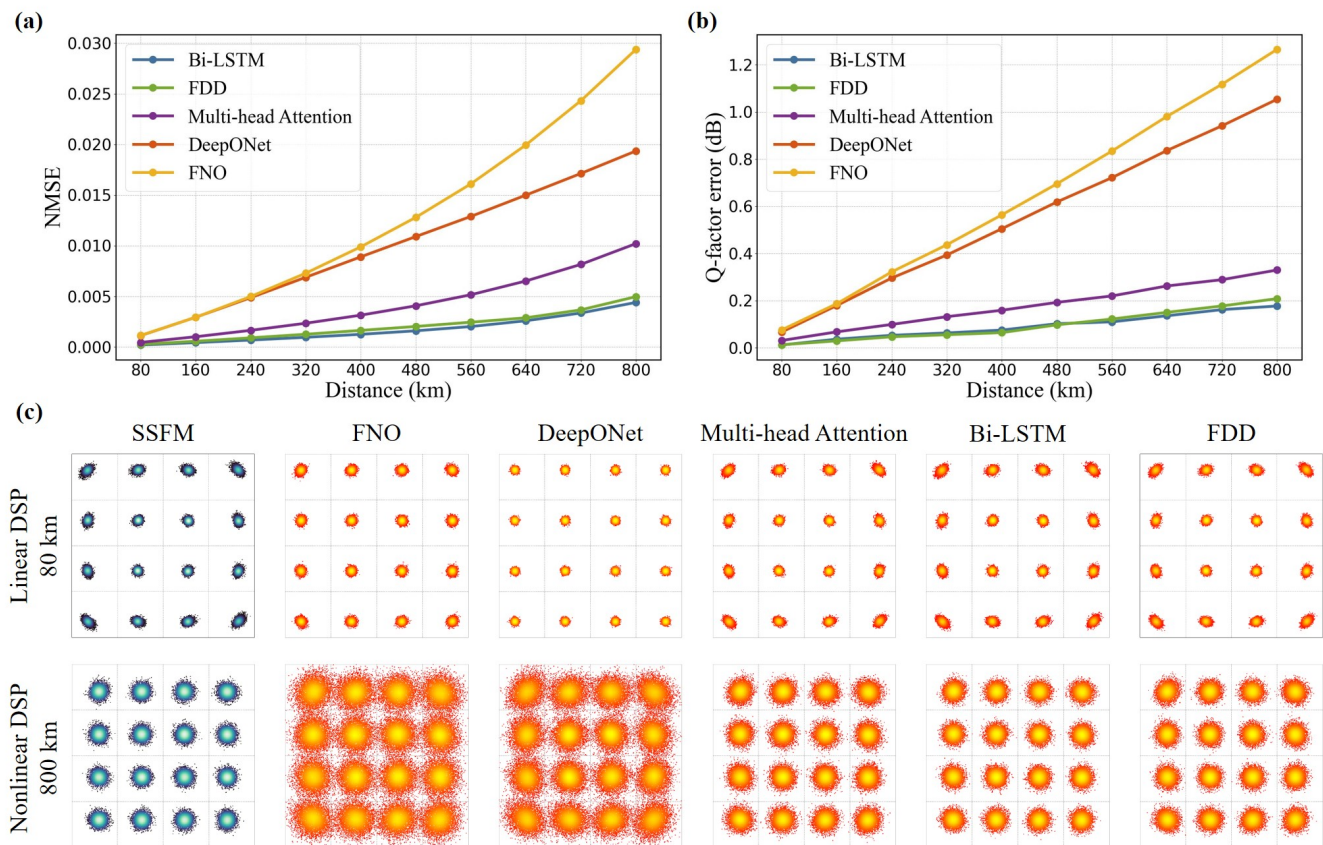


Fig. 7. Comparison of SSFM and DL-based schemes, including pure data-driven schemes and data-physic hybrid-driven schemes. (a) Time-domain waveform of SSFM and DL-based schemes at 800 km. (b) NMSE curve of DL-based schemes covering 800 km. (c) SNR error curve after nonlinear DPS processing between SSFM and DL-based schemes. (d) Constellations after linear DSP processing of SSFM and DL-based schemes at 80 km and 800km.

[33], FNO [32], and DeepONet [42], while the data-physics hybrid-driven scheme is represented by FDD [38]. Pure data-driven schemes model both linear and nonlinear effects, requiring larger input window sizes to account for ISI caused by CD. In contrast, FDD focuses only on nonlinear effects, with linear effects modeled by physical models. This enables FDD to use a shorter input window, determined by formula (7). Thus, pure data-driven schemes utilize an input window

of 165 symbols (82+1+82), whereas the data-physics hybrid-driven scheme requires only 45 symbols (22+1+22). Other model parameters are summarized in Table V.

To evaluate performance, each model is tested over 10 iterations for an 800 km transmission distance and compared to traditional SSFM. Waveform errors are assessed using NMSE. As shown in Fig. 7(a), both FDD and BiLSTM exhibit excellent waveform modeling capabilities, with NMSE values below 5E-

3 over the entire 800 km transmission. Multi-head attention performs slightly worse, with NMSE values just below $1\text{E-}2$, indicating a slight accuracy drop compared to BiLSTM and FDD. FNO and DeepONet exhibit larger discrepancies, with NMSE values of $2.94\text{E-}2$ and $1.94\text{E-}2$, respectively, at 800 km. Notably, FNO's error is six times higher than FDD's at 800 km transmission, indicating significant waveform distortion. The overall waveform modeling accuracy ranks as follows: $\text{FDD} \approx \text{BiLSTM} < \text{Multi-head attention} < \text{DeepONet} < \text{FNO}$, highlighting the superior waveform modeling performance of FDD and BiLSTM.

The QoT errors of each model are evaluated through constellations and Q-factor errors. The first row of Fig. 7(c) presents the constellations of the DL models and SSFM at 80 km transmission after linear DSP. The SSFM constellation shows clear nonlinear phase rotation due to the 4.0 dB launch power, which induces strong nonlinear effects. The constellations of BiLSTM, FDD, and Multi-head Attention display similar nonlinear phase rotations, closely resembling SSFM. However, FNO and DeepONet exhibit Gaussian-like distributions, ignoring nonlinear phase rotation, indicating their worse nonlinear fitting capacity. To further evaluate nonlinear noise distributions at long-haul transmission, the second row of Fig. 7(c) exhibits the constellations at 800 km transmission after nonlinear DSP. After multi-channel DBP, the SSFM constellation shows effective compensation for linear and nonlinear impairments. FDD, BiLSTM, and Multi-head Attention constellations are similarly compensated, although Multi-head Attention shows higher noise than BiLSTM and FDD, reflecting weaker nonlinear modeling. In contrast, FNO and DeepONet constellations exhibit substantial additional noise, indicating severe underfitting of nonlinearities. Subsequently, to quantitatively assess QoT errors, the Q-factor errors compared to SSFM after nonlinear across 800 km transmission are presented in Fig. 7(b). Q-factor errors for all DL models increase with transmission distance, consistent with NMSE trends. BiLSTM and FDD show nearly identical Q-factor errors, with a maximum error of around 0.2 dB compared to SSFM after 800 km transmission, indicating excellent QoT accuracy. Multi-head Attention performs slightly worse, with a maximum Q-factor error of 0.33 dB after 800 km transmission, reflecting its weaker nonlinear fitting capacity. FNO and DeepONet show rapid increases in Q-factor errors, reaching 1.27 dB and 1.05 dB, respectively, indicating substantial inaccuracies in nonlinear modeling.

Results from NMSE, constellations and Q-factor errors show strong consistency, validating the effectiveness and fairness of the DSP-assisted accuracy evaluation method. The ranking of DL schemes in terms of accuracy is: $\text{FDD} \approx \text{BiLSTM} < \text{Multi-head attention} < \text{FNO} < \text{DeepONet}$. The superior performance of FDD, BiLSTM and Multi-head Attention can be attributed to their recurrent structures and multi-head self-attention mechanisms, efficiently capturing temporal correlations of the input signal. FNO and DeepONet, which mainly rely on fully connected and convolutional structures, perform well in single-channel systems but struggle in 5-channel WDM systems. The increased inter-symbol correlations and complex linear and nonlinear couplings in 5-

channel configurations degrade their accuracy. Additionally, fully connected structures face challenges in training and convergence due to the high-dimensional input vector (165 symbols concatenated into a one-dimensional input with a dimensional of 13200). Temporal models like BiLSTM and Multi-head Attention process inputs as two-dimensional vector, with rows representing different time steps. This structure allows the input to be processed step-by-step through recurrent or attention units, reducing neuron dimensionality and mitigating convergence issues inherent to fully connected architectures. Consequently, temporal network architectures outperform fully connected and convolutional networks in multi-channel scenarios. While all five DL models hold potential for accuracy improvement through hyperparameter optimization. However, achieving optimal configurations requires significant effort and is beyond the scope of this study. Nevertheless, the insights derived here provide valuable direction for future advancements in DL-based optical fiber channel modeling.

B. Comparisons in more complex WDM systems

In a 5-channel WDM configuration, BiLSTM and FDD demonstrate comparable performance in waveform and QoT accuracy. To further differentiate their capabilities, we evaluate their performance in more complex WDM scenarios with larger channel counts and higher transmission rates. These test cases include: a 13-channel WDM system with a 50 GBaud transmission rate and 4.0 dBm launch power, and a 5-channel with a 100 GBaud transmission rate and 6.5 dBm launch power. For the 100 GBaud the launch power is increased to 6.5 dBm to match the optimal launch power for higher transmission rates. In these scenarios, the ISI length and nonlinear correlation lengths grow, as determined by equation 6 and 7. Accordingly, input window lengths are set to 427 and 117 symbols for BiLSTM and FDD in the 13-channel 50 GBaud case, and to 601 and 163 symbols in the 5-channel 100 GBaud case.

Both FDD and BiLSTM are tested over 10 iterations to achieve 800 km transmission. Waveform errors are analyzed using NMSE over the 800 km transmission, as shown in Fig. 8(a). In both WDM configurations, FDD consistently outperform BiLSTM, achieving lower NMSE values across 800 km transmission. In the 13-channel 50 GBaud case with 800 km transmission, FDD achieves a maximum NMSE of $1.53\text{E-}2$, compared to BiLSTM's $5\text{E-}2$, resulting in an NMSE difference of $3.47\text{E-}2$. Similarly, in the 5-channel 100 GBaud case, FDD achieves a maximum NMSE of $7\text{E-}3$, significantly lower than BiLSTM's $3.89\text{E-}2$. These results highlight FDD's superior waveform modeling accuracy in more complex WDM configurations.

The QoT errors are evaluated using constellation analysis and Q-factor. The first row of Fig. 8(c) shows that FDD and SSFM constellations exhibit significant nonlinear phase rotation, indicating that FDD effectively captures nonlinearities. Conversely, BiLSTM constellation displays Gaussian-like distributions, failing to replicate nonlinear phase rotation and exposing its limitations in nonlinear modeling. The second row of Fig. 8(c) shows constellations after 800 km

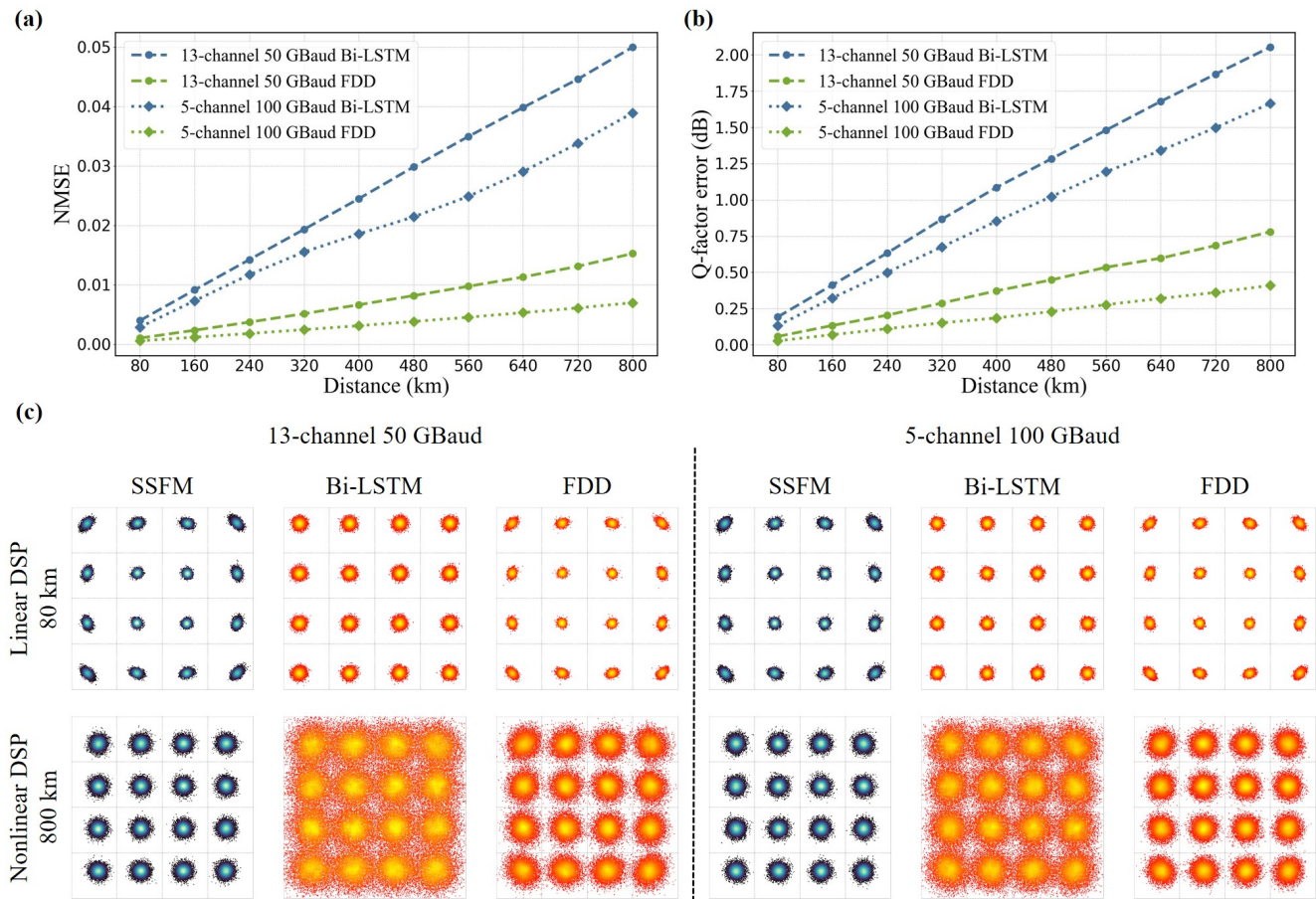


Fig. 8. Comparison of SSFM and FDD under 13-channel with 50 GBaud and 5-channel with 100 GBaud. (a) NMSE curve of FDD covering 800 km. (b) Q-factor errors curve after nonlinear DPS between SSFM and FDD. (c) Constellations after linear DSP at 80 km and after nonlinear DSP at 800 km of SSFM and FDD.

transmission with nonlinear DSP. After multi-channel DBP, SSFM constellations show effective compensation for linear and nonlinear impairments. FDD constellations also achieve strong compensation but display slight additional nonlinear impairments compared to SSFM, indicating minor nonlinear fitting inaccuracies. BiLSTM constellations, however, exhibit significant deviations and additional impairments, rendering BiLSTM ineffective for long-haul transmission. Further, we quantitatively evaluate QoT errors according to Q-factor errors. Fig. 8(b) illustrates the Q-factor errors after nonlinear DSP align with NMSE trends. In the 13-channel 50 GBaud case, FDD achieves a Q-factor error of 0.78 dB after 800 km transmission, compared to 2.05 dB for BiLSTM. Similarly, in the 5-channel 100 GBaud case, FDD achieves a Q-factor error of 0.41 dB, while BiLSTM reaches 1.67 dB, highlighting its substantial performance degradation in high-rate scenarios. These results confirm FDD's robustness and accuracy in both waveform and QoT modeling under complex WDM conditions.

Under more complex large-channel and high-rate WDM configurations, FDD consistently outperforms BiLSTM due to its data-physics hybrid-driven design. FDD separates linear and nonlinear effects, modeling linear effects with a physical model to ensure high linear modeling accuracy across diverse

WDM configurations. This allows the DL model to focus exclusively on residual nonlinearities, simplifying the fitting process, particularly in scenarios with larger channels and higher transmission rates. Additionally, FDD requires a smaller input window than BiLSTM, as the inter-symbol correlations in residual nonlinearities are shorter than in linear effects. This reduces model size, computational resource requirements, and enhance accuracy. In contrast, BiLSTM struggles with large input windows in high-ISI scenarios, leading to degraded performance. As WDM systems grow more complex, ISI effects extend to thousands of symbols, challenging non-decoupling schemes like BiLSTM. FDD's decoupled approach mitigates this challenge, maintaining robust performance.

In conclusion, FDD emerges as the most accurate and efficient DL scheme for large-channel and high-rate WDM scenarios. These results highlight the superiority of data-physics hybrid-driven schemes over pure data-driven schemes and emphasize the importance of integrating physical knowledge in extending DL models to wideband WDM systems.

C. Extending FDD to wideband WDM systems

In the previous section, the FDD scheme demonstrate excellent modeling capabilities, outperforming other DL-based approaches. However, accuracy degradation is observed in

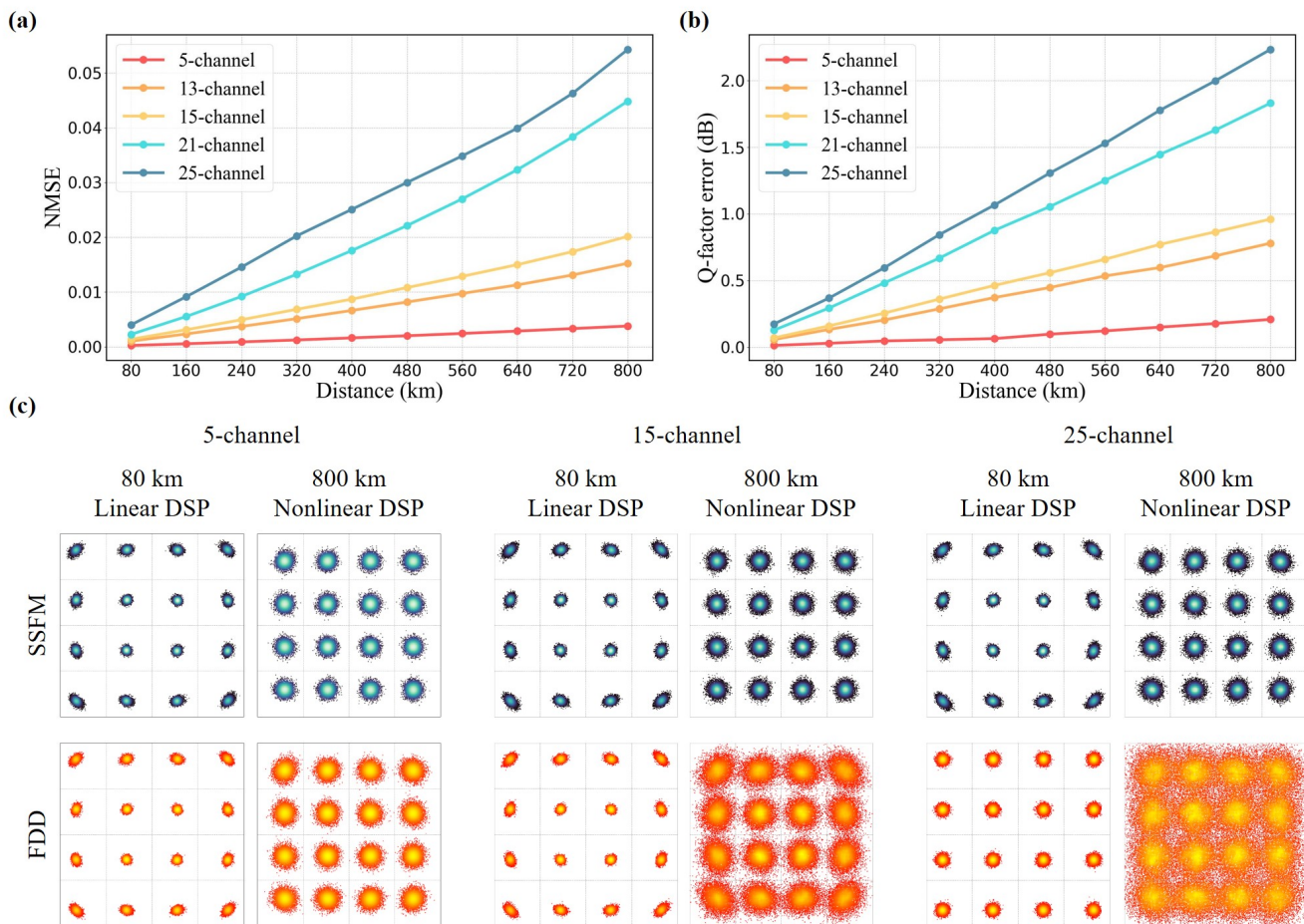


Fig. 9. The results of FDD-BiLSTM applied in larger channels WDM systems. (a) NMSE curve of different number of channels covering 800 km transmission. (b) SNR error curve after nonlinear DSP processing between FDD-BiLSTM and SSFM of different number of channels covering 800 km transmission. (c) Constellations after linear DSP processing of FDD-BiLSTM and SSFM of different number of channels at 80 km and 800 km transmission.

more complex WDM configurations with larger channels and higher transmission rates. In this section, we extend the analysis to evaluate the performance of the FDD scheme under wideband WDM configurations, with up to 25 channels and a transmission rate of 200 GBaud.

1) *Larger-channel WDM systems:* To evaluate the modeling performance of FDD in larger-channel WDM configurations, tests are conducted using channel configurations of [5, 13, 15, 21, 25], with a fixed transmission rate of 50 GBaud, and a launch power of 4 dBm per channel. Results from the previously analyzed 5-channel and 13-channel configurations are included for comparison. As the number of channels increases, signal bandwidth expands, necessitating adjustments to FDD's input window lengths. Based on formula (7), the input window lengths are adjusted to [45, 117, 135, 187, 223] symbols to account for nonlinear inter-symbol correlation in various scenarios.

The NMSE performance of FDD across various channel configurations over an 800 km transmission is shown in Fig. 9(a). After 800 km transmission, the NMSE is just $3.8\text{E-}3$ for 5-channel configuration, compared to $4.49\text{E-}2$ for 21-channel and $5.43\text{E-}2$ for 25-channel configurations—approximately an order of magnitude higher than the 5-channel case—indicating

significant waveform errors in larger-channel scenarios. Further analysis of QoT errors is conducted using constellations and Q-factor errors. First row of Fig. 9(c) shows constellations after 80 km transmission with linear DSP. The nonlinear phase rotation is clearly demonstrated in the constellations for the 5-channel and 15-channel configurations, indicating significant nonlinear modeling capacity of FDD. However, in the 25-channel configuration, the constellations exhibit Gaussian-like distributions and neglect nonlinear characteristic, indicating a severe decline in nonlinear modeling accuracy of FDD. The second row of Fig. 9(c) illustrates constellations after 800 km transmission with nonlinear DSP. Additional nonlinear impairments introduced by the multi-channel DBP algorithm become increasingly apparent with a growing number of channels, indicating weaker nonlinear modeling capacity. As shown in Fig. 9(b), Q-factor errors after nonlinear DSP between SSFM and FDD increase with the number of channels. For the 5-channel scenario, the Q-factor error is 0.21 dB after 800 km transmission, compared to 2.23 dB in the 25-channel configuration—a tenfold increase, indicating more performance gap in larger channel configurations.

The NMSE, constellations, and Q-factor errors collectively indicate accuracy degradation for FDD as the number of

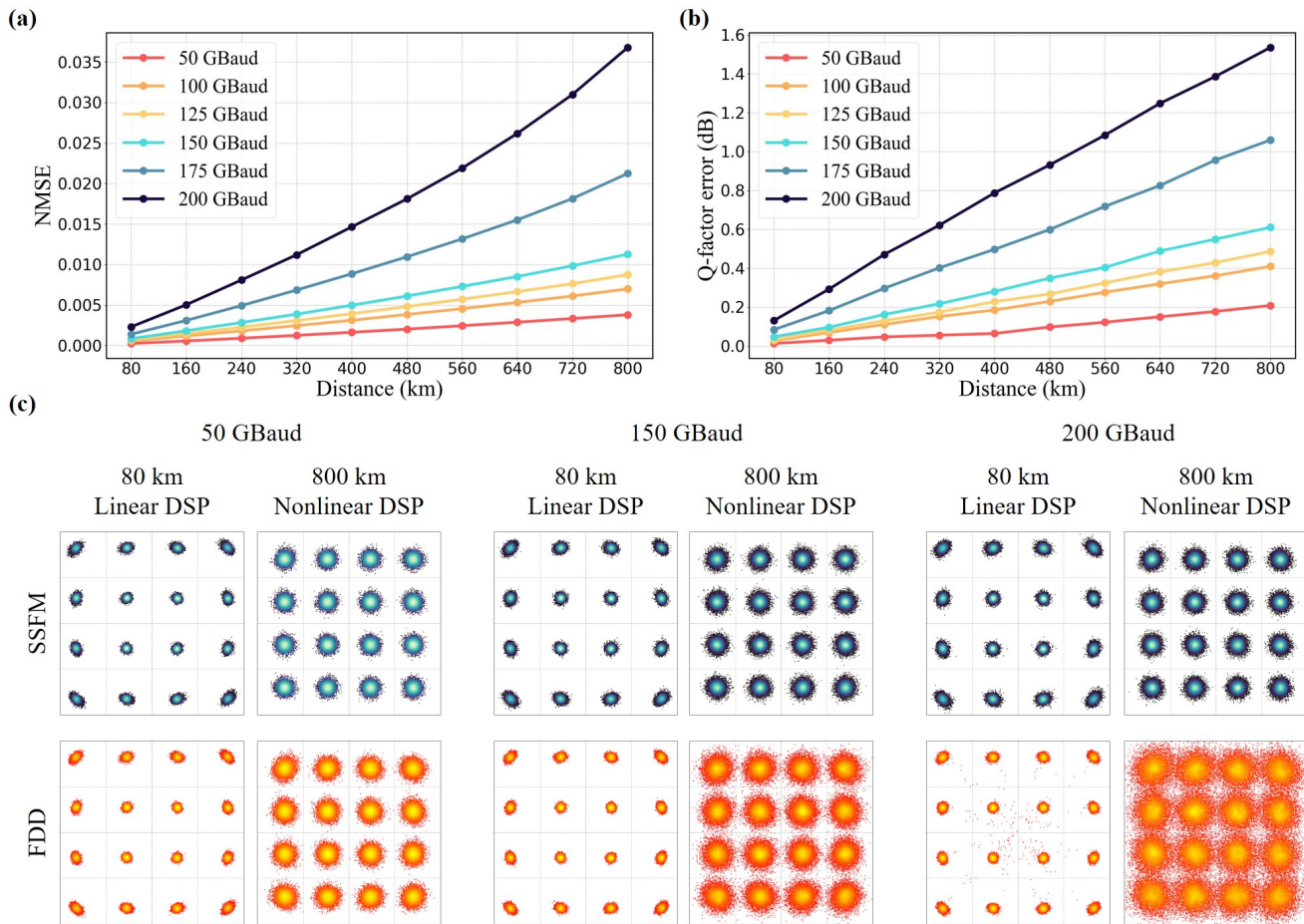


Fig. 10. The results of FDD-BiLSTM applied in higher transmission rates WDM systems. (a) NMSE curve of different transmission rates covering 800 km transmission. (b) SNR error curve after nonlinear DSP processing between FDD-BiLSTM and SSFM of different transmission rates covering 800 km transmission.

channels increases. Several factors contribute to this decline including increased linearity, nonlinearity, and the number of sampling points. Linear effects, primarily caused by CD, results in ISI, which grows with signal bandwidth in larger-channel configurations as described by formula (6). Nonlinear inter-symbol correlations expand alongside ISI, requiring longer input windows of NNs to accommodate these effects. For FDD, this increase necessitates more LSTM cells to process increased input window length, which degrades accuracy for capturing long-term memory [1]. Nonlinear effects in WDM systems, including intra-channel and inter-channel nonlinearities, as described by the equation:

$$\frac{\partial E_k}{\partial z} = -j\gamma_k \left(|E_k|^2 E_k + 2 \sum_{m \neq k} |E_m|^2 E_k + \sum_{n, l, m \in \mathcal{H}} E_n(z, t) E_l(z, t) E_m^*(z, t) e^{j\Delta\beta_{j\text{lim}} z} \right), \quad (14)$$

where the first term on the right represents intra-channel nonlinearity, referred to SPM, and the second and third terms account for inter-channel nonlinearities, referred to XPM and FWM. In larger-channel configurations, inter-channel nonlinear intensifies, imposing greater demands on nonlinear

fitting capabilities of DL models. Additionally, full-filled multi-channel WDM signals requires single-channel signals with higher upsampling points and larger bandwidth to be multiplexed in the frequency domain. Consequently, the input and hidden layer dimension of LSTM cells scale proportionally with the number of channels, expanding the model size. While larger models may offer improved nonlinear representation, they require more data and longer training times to converge. In this study, datasets and training times are not scaled to accommodate the increased model size due to resource constraints. This restricts FDD's performance in larger-channel scenarios, where additional training resources could potentially mitigate some of the observed degradation.

2) *Higher-rate WDM systems*: To evaluate the modeling performance of FDD in higher-rate WDM configurations, tests are conducted using transmission rate configurations of [50, 100, 125, 150, 175, 200] GBaud, with a fixed channel number of 5. The optimize launch power is increased for higher transmission rates, as the nonlinearity is suppressed due to the stronger CD. The launch power for testing is increased with the optimize launch power, about 3 dBm higher than optimize launch power, detailed in Table. VI. Due to the increase of the transmission rate, the signal bandwidth of

TABLE VI
LAUNCH POWER OF VARIOUS TRANSMISSION RATES

Transmission rate (GBaud)	Optimal power (dBm)	Testing power (dBm)
50	1.0	4.0
100	3.5	6.5
125	4.25	7.25
150	5.0	8.0
175	6.75	9.75
200	7.5	10.5

WDM increases with the increase, causing an exponential increase in the nonlinear correlation according to Eq. 7, so the input window length is adjusted to [45, 163, 251, 357, 499, 651] to adapt to this change.

The NMSE performance of FDD across various transmission rate configurations over an 800 km transmission is shown in Fig. 10(a). After 800 km transmission, the NMSE increases with transmission rates, which is just $3.8E-3$ for 50 GBaud configuration, compared to $2.12E-2$ for 175 GBaud and $3.68E-2$ for 200 GBaud configurations, indicating significant waveform errors in higher-rate scenarios. Further analysis of QoT errors is conducted using constellations and Q-factor errors. Fig. 10(c) shows constellations after 80 km transmission with linear DPS and 800 km transmission with nonlinear DSP. First row of each configuration shows that the trend of nonlinear phase rotation of FDD compared to SSFM gradually shows a deviation as the rate increases. Second row of each configuration shows additional nonlinear impairments introduced by the multi-channel DBP algorithm become increasingly apparent with a growing transmission rates. These results from constellations demonstrate weaker nonlinear modeling capacity of FDD in higher-rate configurations. As shown in Fig. 10(b), Q-factor errors after nonlinear DSP between SSFM and FDD increase with the number of channels. For the 50 GBaud scenario, the Q-factor error is 0.21 dB after 800 km transmission, compared to 1.53 dB in the 200 GBaud configuration, indicating more performance gap in higher rate configurations.

The NMSE, constellations, and Q-factor errors collectively indicate accuracy degradation for FDD as the transmission rate increases. Several factors contribute to this decline including increased linearity and nonlinearity. The linear effect is affected by the increase of bandwidth and signal rate in high-speed scenarios, and ISI will show an exponential growth trend. This makes the length of the model input window show a trend of rapid growth, so that Bi-LSTM needs to learn very long pre-and post-correlation, which makes the model accuracy decrease. The enhancement of nonlinear effects in high-speed scenarios is mainly caused by the increase of signal power, since the trend of optimal transmit power growth needs to be satisfied. DL model usually has a decrease in modeling accuracy when it has high power and strong nonlinearity.

In conclusion, the modeling performance of FDD deteriorates in larger-channel WDM configurations due to increased

linearity, nonlinearity, and the number of sampling points. Although FDD remains more accurate than other DL schemes in few-channel scenarios, these findings highlight the challenges of scaling DL-based optical fiber channel modeling to wideband scenarios. Addressing these limitations will be crucial for extending applicability of DL-based schemes to highly complex wideband WDM systems.

VI. POTENTIAL SOLUTION

The performance of DL-based optical fiber channel modeling deteriorates in wideband WDM systems as the number of channels and transmission rates increase, posing significant challenges for their deployment in next-generation optical fiber transmission systems. To address these challenges, three key strategies show substantial potential: standardized accuracy evaluation methods, further decoupling scheme designs, and enhancing in DL model architectures.

A. Standardized accuracy evaluation method

A fair and comprehensive standardized accuracy evaluation method is essential for comprising the performance of various DL models and guiding optimization efforts. In Section III, we introduce a DSP-assisted accuracy evaluation method that evaluates accuracy across two dimensions: waveform error and QoT error. NMSE serves as the metric for waveform errors, while QoT errors are assessed using constellations and Q-factor errors. To address the issue of “anomalous QoT fluctuations” observed after linear DSP, the multi-channel DBP algorithm is employed to provide effective QoT error evaluations. Results presented in Section III and IV demonstrate consistent outcomes across NMSE, constellation, and Q-factor errors, validating the fairness and effectiveness of this method for both narrowband and wideband scenarios. This evaluation method provides a critical benchmark for comparing DL model performance and guiding further optimization.

B. Further decoupling scheme design

Pure data-driven optical fiber channel modeling schemes, relying solely on DL models as “black box” structures, encounter substantial limitations in wideband WDM systems. In contrast, data-physic hybrid-driven scheme, such as FDD, achieve higher accuracy in complex WDM configurations by decoupling linear and nonlinear effects. Linear decoupling allows DL models to concentrate on learning nonlinear effects with shorter inter-symbol correlations, improving accuracy and reducing complexity. Similarly, PINO [35] incorporates the NLSE into the training loss function, reducing dataset requirements and enhancing accuracy. Results [68] show that FDD minimizes NLSE-constrained loss functions more effectively than non-decoupling methods, as shown in Fig. 10. Both FDD and PINO exhibit comparable performance in optimizing NLSE-constrained loss functions. However, these data-physic hybrid-driven schemes require further refinement to achieve optimal accuracy in larger-channel, higher-rate WDM configurations. Additional decoupling strategies, such as nonlinearity decoupling and dynamic linearity decoupling, offer promising avenues for improvement.

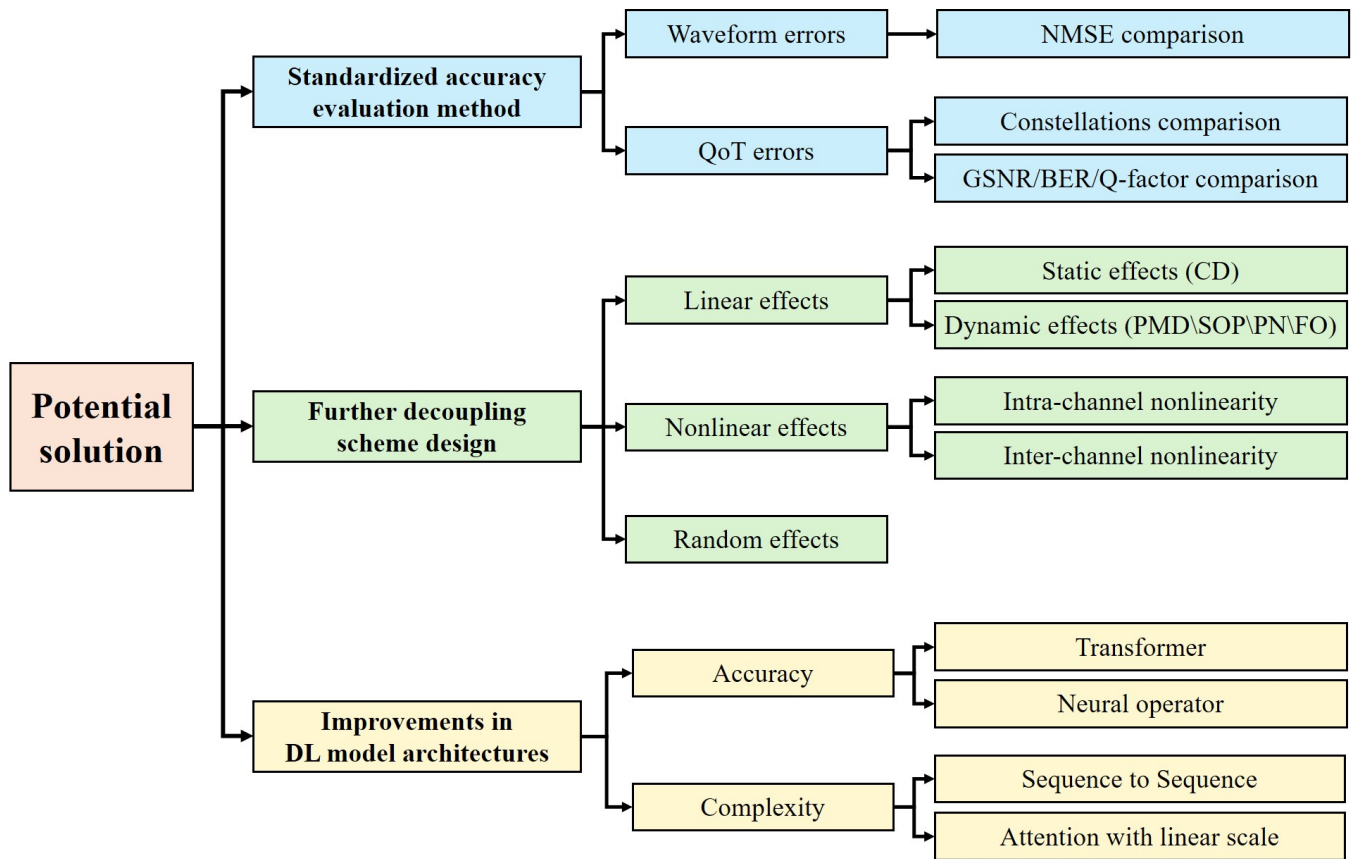


Fig. 11. Potential solution.

Optical fiber nonlinearities comprise intra-channel and inter-channel nonlinearities, offering valuable insights for designing nonlinear decoupling strategies. For instance, a recent approach employing multiple neural networks to separately address intra-channel and inter-channel nonlinearities across various subcarriers [69] demonstrated improved accuracy by reducing the learning complexity for each network. Similarly, stacked DeepONet structures [42] have been employed for optical fiber channel modeling in WDM systems covering the C + L band. The method leverages multiple DeepONets to fit intra-channel nonlinearities for each WDM channel, enabling simultaneous multi-channel signal modeling. Compared to using a single DeepONet for all-channel signals, this approach significantly improves accuracy, making it suitable for wideband WDM systems. Although inter-channel nonlinearities are not considered, this method offers a promising idea for further scheme designs. Leveraging distinct neural networks to separately model intra-channel and inter-channel nonlinearities offers a promising strategy to mitigate the challenges of using a single NN to capture both intra- and inter-channel nonlinearities, especially in wideband WDM systems.

To better align with real-world optical transmission systems, optical fiber simulation models must account for dynamic linearities, including SOP, PMD, phase noise (PN) and frequency offset (FO). These dynamic linearities with time-varying features pose significant challenges for DL models, which primarily suited to capturing deterministic responses. Advanced DSP

algorithms based on physical models, such as MIMO, LOFO, and CPR, excel in managing dynamic linear impairments. A digital twin (DT) framework proposed in [70] integrates these DSP algorithms with DL models to mirror real optical fiber transmission systems. In this framework, DSP algorithms decouple dynamic linearity, generating labels that retain only residual deterministic effects for training NNs. This innovative DT framework addresses the challenges posed by capturing dynamic linearities in DL models and lays the groundwork for developing DL-based schemes that incorporate dynamic linear effects.

C. Enhancing DL model architectures

Further advancements in DL-based optical fiber channel modeling focus on enhancing model architectures to improve nonlinear fitting capabilities and reduce computational complexity.

In wideband WDM systems, intricate inter-channel nonlinearities coupling imposes stringent demands on the nonlinear fitting capabilities of DL models. Studies [71] have demonstrated a direct correlation between the number of parameters in a DL model and its accuracy, suggesting that increasing model parameters can improve performance. However, for architectures like LSTM, increasing depth may lead to diminishing returns due to performance bottlenecks []. The Transformer architecture [72], leveraging multi-head attention mechanisms, has recently demonstrated exceptional scalability,

supporting models with tens of billions of parameters, as seen in large language models (LLMs) [73]–[75]. Within the range of such parameters, a positive relationship between parameters count and performance has been established, with emergent capabilities arising beyond specific threshold [71]. Consequently, designing DL schemes based on the multi-head attention offers a promising direction for scaling parameters to address more complex nonlinear modeling tasks. For instance, an Encoder-only Transformer [39] combined with FDD outperformed BiLSTM for optical channel modeling in a 21-channel WDM system.

Beyond neural networks, neural operators have emerged as a promising direction to their robust generalization capabilities [76], [77]. While earlier results show that DeepONet and FNO have yet to achieve outstanding performance, their primary limitation stem from their fully connected architectures, which are less effective for wideband WDM systems requiring extended input windows to address longer ISI. Advanced neural operator designs, such as the Koopman neural operator, offer a potential avenue for optimization. Another promising approach involves integrating temporal architectures into neural operator frameworks. For instance, DeepONet’s trunk and branch network structures are inherently flexible and could be enhanced by replacing fully connected layers with temporal architectures, addressing challenges related to longer ISI. The application of advanced neural operators holds immense potential for improving DL-based optical fiber channel modeling.

Optimizing the complexity of DL models is another critical focus, particularly for wideband WDM systems with longer ISI and extended input window requirements. The Co-LSTM [34] introduced a recycling mechanism during inference, simplifying the complexity of traditional LSTM. For models employing multi-head attention mechanism, complexity scales as $O(N^2)$ with input sequence length, posing challenges for wideband WDM systems. Although little research has directly addressed complexity optimization for multi-head attention in optical fiber channel modeling, advances in other fields provide valuable insights. For instance, the Longformer architecture [78] introduces an attention mechanism that scales linearly with sequence length, enabling efficient processing of inputs with thousands of tokens. Such developments, combined with ongoing research to optimize LSTM and Transformer-like architectures, highlight promising strategies for overcoming complexity constraints in DL-based optical fiber modeling.

In summary, while DL-based waveform-level optical fiber channel modeling schemes face significant accuracy and complexity challenges in wideband WDM systems, advancements in further decoupling scheme design and enhancing of DL models offers a promising pathway forward. With continued advancements, DL approaches are well-positioned to unlock their full potential and achieve broader adoption in wideband WDM systems.

VII. CONCLUSION

DL-based optical fiber channel modeling schemes are expected to outperform the traditional methods like the SSFM due to their enhanced precision and reduced complexity. We

propose a DSP-assisted accuracy evaluation method to address the limitations of traditional accuracy metrics. This evaluation method integrates waveform errors and QoT errors, enabling a detailed evaluation on the accuracy of DL-based schemes. Leveraging advanced linear and nonlinear DSP algorithms, we can analyze the effect of different types of errors on QoT from the perspective of constellations and Q-factor errors aligning with the results of waveform errors, providing a fair and comprehensive accuracy evaluation processing. Furthermore, we review current DL-based waveform modeling schemes, and compare their performance. Results demonstrate that FDD and BiLSTM achieve superior performance among five DL schemes, with a maximal NMSE improvement of 83.1% and a Q-factor error reduction of 1.06 dB in a 5-channel with 50 GBaud configuration. Further tests of FDD in wideband WDM systems with large-channel and high-rate reveal significant performance degradation: NMSE degradation by 92.9%, and Q-factor errors increased by 2.02 dB when scaling from 5 to 25 channels; similarly, NMSE degradation reaches 89.7%, and Q-factor errors rise by 1.33 dB when symbol rates increase from 50 to 200 GBaud. Finally, we analyze the challenges in scaling DL-based waveform-level channel modeling for wideband configurations and propose potential solutions. This study establishes a solid foundation for accuracy evaluation in DL-based optical fiber channel modeling, analyzes the performance of existing schemes, and highlights direction for future research. DL-based efficient and precise simulation tools can break through the limitation of expensive physical devices and accelerate advancement of research into fiber nonlinearities required to explore the channel capacity of nonlinear fibers, thus contributing to the continuous evolution of next-generation optical networks.

ACKNOWLEDGMENTS

The authors acknowledge the funding provided by the National Key R&D Program of China (2023YFB2905400), National Natural Science Foundation of China (62025503), and Shanghai Jiao Tong University 2030 Initiative.

REFERENCES

- [1] E. B. Desurvire, “Capacity demand and technology challenges for lightwave systems in the next two decades,” *Journal of Lightwave Technology*, vol. 24, no. 12, pp. 4697–4710, 2006.
- [2] C. A. of Cyberspace Studies, *Development of Information Infrastructure in the World*. Singapore: Springer Singapore, 2021, pp. 1–23. [Online]. Available: https://doi.org/10.1007/978-981-33-6938-2_1
- [3] P. J. Winzer, D. T. Neilson, and A. R. Chraplyvy, “Fiber-optic transmission and networking: the previous 20 and the next 20 years,” *Opt. Express*, vol. 26, no. 18, pp. 24 190–24 239, Sep 2018. [Online]. Available: <https://opg.optica.org/oe/abstract.cfm?URI=oe-26-18-24190>
- [4] Y. Zhang, X. Pang, Y. Song, Y. Wang, Y. Zhou, H. Zhu, L. Zhang, Y. Fan, Z. Guo, S. Huang, M. Zhang, and D. Wang, “Optical power control for gsnr optimization based on c+l-band digital twin systems,” *J. Lightwave Technol.*, vol. 42, no. 1, pp. 95–105, Jan 2024. [Online]. Available: <https://opg.optica.org/jlt/abstract.cfm?URI=jlt-42-1-95>
- [5] B. Correia, R. Sadeghi, E. Virgillito, A. Napoli, N. Costa, J. Pedro, and V. Curri, “Optical power control strategies for optimized c+l+s-bands network performance,” in *2021 Optical Fiber Communications Conference and Exhibition (OFC)*, 2021, pp. 1–3.
- [6] I. Roberts, J. M. Kahn, J. Harley, and D. W. Boertjes, “Channel power optimization of wdm systems following gaussian noise nonlinearity model in presence of stimulated raman scattering,” *Journal of Lightwave Technology*, vol. 35, no. 23, pp. 5237–5249, 2017.

- [7] Y. Song, Q. Fan, C. Lu, D. Wang, and A. P. T. Lau, "Efficient three-step amplifier configuration algorithm for dynamic c+l-band links in presence of stimulated raman scattering," *Journal of Lightwave Technology*, vol. 41, no. 5, pp. 1445–1453, 2023.
- [8] C. Zhang, D. Wang, J. Jia, L. Wang, K. Chen, L. Guan, Z. Liu, Z. Zhang, X. Chen, and M. Zhang, "Potential failure cause identification for optical networks using deep learning with an attention mechanism," *Journal of Optical Communications and Networking*, vol. 14, no. 2, pp. A122–A133, 2022.
- [9] Y. Zhang, M. Zhang, Y. Song, Y. Shi, C. Zhang, C. Ju, B. Guo, S. Huang, and D. Wang, "Building a digital twin for large-scale and dynamic c+l-band optical networks," *Journal of Optical Communications and Networking*, vol. 15, no. 12, pp. 985–998, 2023.
- [10] A. Napoli, Z. Maalej, V. A. J. M. Sleiffer, M. Kuschnerov, D. Rafique, E. Timmers, B. Spinnler, R. Rahman, L. D. Coelho, and N. Hanik, "Reduced complexity digital back-propagation methods for optical communication systems," *Journal of Lightwave Technology*, vol. 32, no. 7, pp. 1351–1362, 2014.
- [11] O. Vassilieva, I. Kim, and T. Ikeuchi, "Enabling technologies for fiber nonlinearity mitigation in high capacity transmission systems," *Journal of Lightwave Technology*, vol. 37, no. 1, pp. 50–60, 2019.
- [12] Q. Fan, G. Zhou, T. Gui, C. Lu, and A. P. T. Lau, "Advancing theoretical understanding and practical performance of signal processing for nonlinear optical communications through machine learning," *Nature Communications*, vol. 11, p. 3694, 07 2020.
- [13] O. Sidelnikov, A. Redyuk, S. Sygletos, M. Fedoruk, and S. Turitsyn, "Advanced convolutional neural networks for nonlinearity mitigation in long-haul wdm transmission systems," *Journal of Lightwave Technology*, vol. 39, no. 8, pp. 2397–2406, 2021.
- [14] X. Lin, S. Luo, S. K. O. Soman, O. A. Dobre, L. Lampe, D. Chang, and C. Li, "Perturbation theory-aided learned digital back-propagation scheme for optical fiber nonlinearity compensation," *Journal of Lightwave Technology*, vol. 40, no. 7, pp. 1981–1988, 2022.
- [15] B. Karanov, M. Chagnon, F. Thouin, T. A. Eriksson, H. Bülow, D. Lavery, P. Bayvel, and L. Schmalen, "End-to-end deep learning of optical fiber communications," *Journal of Lightwave Technology*, vol. 36, no. 20, pp. 4843–4855, 2018.
- [16] B. Karanov, D. Lavery, P. Bayvel, and L. Schmalen, "End-to-end optimized transmission over dispersive intensity-modulated channels using bidirectional recurrent neural networks," *Opt. Express*, vol. 27, no. 14, pp. 19650–19663, Jul 2019. [Online]. Available: <https://opg.optica.org/oe/abstract.cfm?URI=oe-27-14-19650>
- [17] B. Karanov, M. Chagnon, V. Aref, D. Lavery, P. Bayvel, and L. Schmalen, "Optical fiber communication systems based on end-to-end deep learning : (invited paper)," in *2020 IEEE Photonics Conference (IPC)*, 2020, pp. 1–2.
- [18] Z. Niu, H. Yang, H. Zhao, C. Dai, W. Hu, and L. Yi, "End-to-end deep learning for long-haul fiber transmission using differentiable surrogate channel," *Journal of Lightwave Technology*, vol. 40, no. 9, pp. 2807–2822, 2022.
- [19] Y. Xu, L. Huang, W. Jiang, X. Guan, W. Hu, and L. Yi, "End-to-end learning for 100g-pon based on noise adaptation network," *Journal of Lightwave Technology*, vol. 42, no. 7, pp. 2328–2337, 2024.
- [20] M. Li and S. Wang, "End-to-end learning for chromatic dispersion compensation in optical fiber communication," *IEEE Communications Letters*, vol. 26, no. 8, pp. 1829–1832, 2022.
- [21] J. Song, C. Häger, J. Schröder, A. G. I. Amat, and H. Wymeersch, "Model-based end-to-end learning for wdm systems with transceiver hardware impairments," *IEEE Journal of Selected Topics in Quantum Electronics*, vol. 28, no. 4: Mach. Learn. in Photon. Commun. and Meas. Syst., pp. 1–14, 2022.
- [22] D. Gloge, "Optical fibers for communication," *Appl. Opt.*, vol. 13, no. 2, pp. 249–254, Feb 1974. [Online]. Available: <https://opg.optica.org/ao/abstract.cfm?URI=ao-13-2-249>
- [23] G. P. Agrawal, "Nonlinear fiber optics," in *Nonlinear Science at the Dawn of the 21st Century*, P. L. Christiansen, M. P. Sørensen, and A. C. Scott, Eds. Berlin, Heidelberg: Springer Berlin Heidelberg, 2000, pp. 195–211.
- [24] P. Serena, C. Lasagni, S. Musetti, and A. Bononi, "On numerical simulations of ultra-wideband long-haul optical communication systems," *Journal of Lightwave Technology*, vol. 38, no. 5, pp. 1019–1031, 2020.
- [25] P. Poggiolini, "The gn model of non-linear propagation in uncompensated coherent optical systems," *Journal of Lightwave Technology*, vol. 30, no. 24, pp. 3857–3879, 2012.
- [26] A. Carena, G. Bosco, V. Curri, Y. Jiang, P. Poggiolini, and F. Forghieri, "Egn model of non-linear fiber propagation," *Opt. Express*, vol. 22, no. 13, pp. 16335–16362, Jun 2014. [Online]. Available: <https://opg.optica.org/oe/abstract.cfm?URI=oe-22-13-16335>
- [27] K. Hornik, M. Stinchcombe, and H. White, "Multilayer feedforward networks are universal approximators," *Neural Networks*, vol. 2, no. 5, pp. 359–366, 1989. [Online]. Available: <https://www.sciencedirect.com/science/article/pii/0893608089900208>
- [28] J. Wei, X. Zhang, Z. Ji *et al.*, "Deploying and scaling distributed parallel deep neural networks on the tianhe-3 prototype system," *Scientific Reports*, vol. 11, p. 20244, 2021.
- [29] D. Wang, Y. Song, J. Li, J. Qin, T. Yang, M. Zhang, X. Chen, and A. C. Boucouvalas, "Data-driven optical fiber channel modeling: A deep learning approach," *Journal of Lightwave Technology*, vol. 38, no. 17, pp. 4730–4743, 2020.
- [30] H. Yang, Z. Niu, S. Xiao, J. Fang, Z. Liu, D. Fainsin, and L. Yi, "Fast and accurate optical fiber channel modeling using generative adversarial network," *Journal of Lightwave Technology*, vol. 39, no. 5, pp. 1322–1333, 2021.
- [31] X. He, L. Yan, L. Jiang, A. Yi, Z. Pu, Y. Yu, W. Pan, and B. Luo, "Data-driven optical fiber channel modeling using fourier neural operator," in *2022 Conference on Lasers and Electro-Optics (CLEO)*, 2022, pp. 1–2.
- [32] X. He, L. Yan, L. Jiang, A. Yi, Z. Pu, Y. Yu, H. Chen, W. Pan, and B. Luo, "Fourier neural operator for accurate optical fiber modeling with low complexity," *Journal of Lightwave Technology*, vol. 41, no. 8, pp. 2301–2311, 2023.
- [33] Y. Zang, Z. Yu, K. Xu, M. Chen, S. Yang, and H. Chen, "Multi-span long-haul fiber transmission model based on cascaded neural networks with multi-head attention mechanism," *Journal of Lightwave Technology*, vol. 40, no. 19, pp. 6347–6358, 2022.
- [34] J. Zheng, T. Zhang, and F. Zhang, "Co-lstm-based fiber link modeling with ase noise tracking for long-haul coherent optical transmission," *Opt. Lett.*, vol. 49, no. 7, pp. 1848–1851, Apr 2024. [Online]. Available: <https://opg.optica.org/ol/abstract.cfm?URI=ol-49-7-1848>
- [35] Y. Song, D. Wang, Q. Fan, X. Jiang, X. Luo, and M. Zhang, "Physics-informed neural operator for fast and scalable optical fiber channel modelling in multi-span transmission," in *2022 European Conference on Optical Communication (ECOC)*, 2022, pp. 1–4.
- [36] R. Jiang, Z. Fu, Y. Bao, H. Wang, X. Ding, and Z. Wang, "Data-driven method for nonlinear optical fiber channel modeling based on deep neural network," *IEEE Photonics Journal*, vol. 14, no. 4, pp. 1–8, 2022.
- [37] Q. Qiu, H. Lun, X. Liu, L. Yi, W. Hu, and Q. Zhuge, "Fourier neural operator based fibre channel modelling for optical transmission," in *2022 European Conference on Optical Communication (ECOC)*, 2022, pp. 1–4.
- [38] H. Yang, Z. Niu, H. Zhao, S. Xiao, W. Hu, and L. Yi, "Fast and accurate waveform modeling of long-haul multi-channel optical fiber transmission using a hybrid model-data driven scheme," *Journal of Lightwave Technology*, vol. 40, no. 14, pp. 4571–4580, 2022.
- [39] M. Shi, H. Yang, Z. Niu, C. Zeng, S. Xiao, W. Hu, and L. Yi, "Accurate and efficient optical fiber wdm transmission modeling using the encoder-only transformer with feature decoupling distributed method," in *2023 Asia Communications and Photonics Conference/2023 International Photonics and Optoelectronics Meetings (ACP/POEM)*, 2023, pp. 1–5.
- [40] C. Zeng, Z. Niu, H. Yang, M. Shi, W. Hu, and L. Yi, "Enhancing generalization in neural channel model for optical fiber wdm transmission through learned encoding of system parameters," in *2024 Optical Fiber Communications Conference and Exhibition (OFC)*, 2024, pp. 1–3.
- [41] X. Zhang, D. Wang, Y. Song, X. Jiang, J. Li, and M. Zhang, "Neural operator-based fiber channel modeling for wdm optical transmission system," in *2023 Opto-Electronics and Communications Conference (OECC)*, 2023, pp. 1–4.
- [42] X. Zhang, M. Zhang, Y. Song, X. Jiang, F. Zhang, and D. Wang, "Deepnet-based waveform-level simulation for a wideband nonlinear wdm system," *Journal of Lightwave Technology*, vol. 41, no. 22, pp. 6908–6922, 2023.
- [43] N. Zhang, H. Yang, Z. Niu, L. Zheng, C. Chen, S. Xiao, and L. Yi, "Transformer-based long distance fiber channel modeling for optical ofdm systems," *Journal of Lightwave Technology*, vol. 40, no. 24, pp. 7779–7789, 2022.
- [44] W. Chen, M. Zhang, D. Wang, Y. Zhan, S. Cai, H. Yang, Z. Zhang, X. Chen, and D. Wang, "Deep learning-based channel modeling for free space optical communications," *Journal of Lightwave Technology*, vol. 41, no. 1, pp. 183–198, 2023.
- [45] M. Ma, H. Chang, R. Gao, D. Guo, X. Liu, and M. Yuan, "Modeling of multi-core fiber channel based on m-cgan for high capacity fiber optical communication," in *2023 Asia Communications and Photonics*

- Conference/2023 International Photonics and Optoelectronics Meetings (ACP/POEM)*, 2023, pp. 01–05.
- [46] M. Yuan, H. Chang, M. Ma, R. Gao, F. Wang, Q. Zhang, D. Guo, Z. Li, F. Wang, and X. Huang, “A conditional generative adversarial network aided few-mode fiber channel modeling for large-capacity optical fiber communication,” in *2023 21st International Conference on Optical Communications and Networks (ICOON)*, 2023, pp. 1–3.
- [47] Y. Zhu, J. Ye, L. Yan, T. Zhou, P. Li, X. Zou, and W. Pan, “Transformer-based high-fidelity modeling method for radio over fiber link,” *Journal of Lightwave Technology*, vol. 41, no. 9, pp. 2657–2665, 2023.
- [48] S. Boscolo and C. Finot, “Artificial neural networks for nonlinear pulse shaping in optical fibers,” *Optics & Laser Technology*, vol. 131, p. 106439, 2020.
- [49] T. Zahavy, A. Dikopoltsev, D. Moss, G. I. Haham, O. Cohen, S. Mannor, and M. Segev, “Deep learning reconstruction of ultrashort pulses,” *Optica*, vol. 5, no. 5, pp. 666–673, 2018.
- [50] L. Salmela, N. Tspinkakis, A. Foi, C. Billet, J. M. Dudley, and G. Genty, “Predicting ultrafast nonlinear dynamics in fibre optics with a recurrent neural network,” *Nature machine intelligence*, vol. 3, no. 4, pp. 344–354, 2021.
- [51] H. Yang, H. Zhao, Z. Niu, G. Pu, S. Xiao, W. Hu, and L. Yi, “Low-complexity full-field ultrafast nonlinear dynamics prediction by a convolutional feature separation modeling method,” *Optics Express*, vol. 30, no. 24, pp. 43 691–43 705, 2022.
- [52] U. Teğin, B. Rahmani, E. Kakkava, N. Borhani, C. Moser, and D. Psaltis, “Controlling spatiotemporal nonlinearities in multimode fibers with deep neural networks,” *Appl Photonics*, vol. 5, no. 3, 2020.
- [53] M. Raissi, P. Perdikaris, and G. E. Karniadakis, “Physics-informed neural networks: A deep learning framework for solving forward and inverse problems involving nonlinear partial differential equations,” *Journal of Computational physics*, vol. 378, pp. 686–707, 2019.
- [54] X.-M. Liu, Z.-Y. Zhang, and W.-J. Liu, “Physics-informed neural network method for predicting soliton dynamics supported by complex parity-time symmetric potentials,” *Chinese Physics Letters*, vol. 40, no. 7, p. 070501, 2023.
- [55] S.-Y. Xu, Q. Zhou, and W. Liu, “Prediction of soliton evolution and equation parameters for nls–mb equation based on the phpinn algorithm,” *Nonlinear Dynamics*, vol. 111, no. 19, pp. 18 401–18 417, 2023.
- [56] X. Jiang, D. Wang, Q. Fan, M. Zhang, C. Lu, and A. P. T. Lau, “Solving the nonlinear schrödinger equation in optical fibers using physics-informed neural network,” in *Optical fiber communication conference*. Optica Publishing Group, 2021, pp. M3H–8.
- [57] D. Wang, X. Jiang, Y. Song, M. Fu, Z. Zhang, X. Chen, and M. Zhang, “Applications of physics-informed neural network for optical fiber communications,” *IEEE Communications Magazine*, vol. 60, no. 9, pp. 32–37, 2022.
- [58] X. Jiang, D. Wang, Q. Fan, M. Zhang, C. Lu, and A. P. T. Lau, “Physics-informed neural network for nonlinear dynamics in fiber optics,” *Laser & Photonics Reviews*, vol. 16, no. 9, p. 2100483, 2022.
- [59] G. Genty, L. Salmela, J. M. Dudley, D. Brunner, A. Kokhanovskiy, S. Kobtsev, and S. K. Turitsyn, “Machine learning and applications in ultrafast photonics,” *Nature Photonics*, vol. 15, no. 2, pp. 91–101, 2021.
- [60] C. Menyuk, “Nonlinear pulse propagation in birefringent optical fibers,” *IEEE Journal of Quantum Electronics*, vol. 23, no. 2, pp. 174–176, 1987.
- [61] D. Marcuse, C. Menyuk, and P. Wai, “Application of the manakov-pmd equation to studies of signal propagation in optical fibers with randomly varying birefringence,” *Journal of Lightwave Technology*, vol. 15, no. 9, pp. 1735–1746, 1997.
- [62] S. Evangelides, L. Mollenauer, J. Gordon, and N. Bergano, “Polarization multiplexing with solitons,” *Journal of Lightwave Technology*, vol. 10, no. 1, pp. 28–35, 1992.
- [63] O. Sinkin, R. Holzlohner, J. Zweck, and C. Menyuk, “Optimization of the split-step fourier method in modeling optical-fiber communications systems,” *Journal of Lightwave Technology*, vol. 21, no. 1, pp. 61–68, 2003.
- [64] E. Ip and J. M. Kahn, “Compensation of dispersion and nonlinear impairments using digital backpropagation,” *Journal of Lightwave Technology*, vol. 26, no. 20, pp. 3416–3425, 2008.
- [65] L. Mescheder, S. Nowozin, and A. Geiger, “The numerics of gans,” in *Proceedings of the 31st International Conference on Neural Information Processing Systems*, ser. NIPS’17. Red Hook, NY, USA: Curran Associates Inc., 2017, p. 1823–1833.
- [66] A. Mecozzi, C. Clausen, and M. Shtaif, “Analysis of intrachannel nonlinear effects in highly dispersed optical pulse transmission,” *IEEE Photonics Technology Letters*, vol. 12, no. 4, pp. 392–394, 2000.
- [67] J. Gui, Z. Sun, Y. Wen, D. Tao, and J. Ye, “A review on generative adversarial networks: Algorithms, theory, and applications,” 2020. [Online]. Available: <https://arxiv.org/abs/2001.06937>
- [68] Y. Zhang, Z. Niu, M. Shi, W. Hu, and L. Yi, “Improve the fitting accuracy of deep learning for the nonlinear schrödinger equation using linear feature decoupling method,” in *2024 Asia Communications and Photonics Conference (ACP) and International Conference on Information Photonics and Optical Communications (IPOC)*, 2024, pp. 1–4.
- [69] A. Bakhshali, H. Najafi, B. B. Hamgini, and Z. Zhang, “Neural network architectures for optical channel nonlinear compensation in digital subcarrier multiplexing systems,” *Opt. Express*, vol. 31, no. 16, pp. 26 418–26 434, Jul 2023. [Online]. Available: <https://opg.optica.org/oe/abstract.cfm?URI=oe-31-16-26418>
- [70] H. Yang, Z. Niu, Q. Fan, L. Li, M. Shi, C. Zeng, S. Xiao, W. Hu, and L. Yi, “The digital twin framework for the physical wideband and long-haul optical fiber communication systems,” *Laser & Photonics Reviews*, vol. n/a, no. n/a, p. 2400234. [Online]. Available: <https://onlinelibrary.wiley.com/doi/abs/10.1002/lpor.202400234>
- [71] J. Kaplan, S. McCandlish, T. Henighan, T. B. Brown, B. Chess, R. Child, S. Gray, A. Radford, J. Wu, and D. Amodei, “Scaling laws for neural language models,” 2020. [Online]. Available: <https://arxiv.org/abs/2001.08361>
- [72] A. Vaswani, N. Shazeer, N. Parmar, J. Uszkoreit, L. Jones, A. N. Gomez, L. Kaiser, and I. Polosukhin, “Attention is all you need,” 2023. [Online]. Available: <https://arxiv.org/abs/1706.03762>
- [73] J. Devlin, M.-W. Chang, K. Lee, and K. Toutanova, “Bert: Pre-training of deep bidirectional transformers for language understanding,” 2019. [Online]. Available: <https://arxiv.org/abs/1810.04805>
- [74] T. B. Brown, B. Mann, N. Ryder, M. Subbiah, J. Kaplan, P. Dhariwal, A. Neelakantan, P. Shyam, G. Sastry, A. Askell, S. Agarwal, A. Herbert-Voss, G. Krueger, T. Henighan, R. Child, A. Ramesh, D. M. Ziegler, J. Wu, C. Winter, C. Hesse, M. Chen, E. Sigler, M. Litwin, S. Gray, B. Chess, J. Clark, C. Berner, S. McCandlish, A. Radford, I. Sutskever, and D. Amodei, “Language models are few-shot learners,” in *Proceedings of the 34th International Conference on Neural Information Processing Systems*, ser. NIPS ’20. Red Hook, NY, USA: Curran Associates Inc., 2020.
- [75] —, “Language models are few-shot learners,” 2020. [Online]. Available: <https://arxiv.org/abs/2005.14165>
- [76] Z. Li, N. Kovachki, K. Azizzadenesheli, B. Liu, K. Bhattacharya, A. Stuart, and A. Anandkumar, “Fourier neural operator for parametric partial differential equations,” 2021. [Online]. Available: <https://arxiv.org/abs/2010.08895>
- [77] L. Lu, P. Jin, G. Pang, and G. E. Karniadakis, “Learning nonlinear operators via deeponet based on the universal approximation theorem of operators,” *Nature Machine Intelligence*, vol. 3, no. 3, pp. 218–229, 2021. [Online]. Available: <https://doi.org/10.1038/s42256-021-00302-5>
- [78] I. Beltagy, M. E. Peters, and A. Cohan, “Longformer: The long-document transformer,” 2020. [Online]. Available: <https://arxiv.org/abs/2004.05150>